



**Utrecht
University**



UMC Utrecht

Developing human in vitro models for SARS-CoV-2 infection to more closely resemble the in vivo situation.

Liset de Vries

Major research project October 2020-September 2021

Virology department of Medical Microbiology

UMC Utrecht, the Netherlands

Master Infection and Immunity

Utrecht University

Daily supervisor: Dr. Patrique Praest
Examiner: Dr. Robert Jan Lebbink
Second reviewer: Dr. Frank Coenjaerts

Abbreviations:

- ACE2: Angiotensin Converting Enzyme 2
- BSL3: biosafety level 3
- COVID-19: coronavirus disease 2019
- DIP: defective interfering particles
- DPI: days post-infection
- EMA: European medicines agency
- FDA: food drug administration
- HR: heptat repeats
- HNEC: Human Nasal Epithelial Cells
- ICU: Intensive Care unit
- MERS-CoV: Middle East Respiratory Syndrome Coronavirus
- NGFR: nerve growth factor receptor
- RBD: receptor binding domain
- RTC: replication/transcription complex
- SARS-CoV: Severe Acute Respiratory Syndrome Coronavirus
- SARS-CoV-2: Severe acute respiratory syndrome coronavirus 2
- TMPRSS2: transmembrane protease/serine subfamily member 2

Abstract

The SARS-CoV-2 pandemic has taken over 4 million lives over the world and impacted countless others. Despite therapeutic strategies and vaccines being developed, cases continue to rise and the end of the pandemic seems to be far from now. For this reason, new insights into the biology of SARS-CoV-2 and new strategies to manage and fight the virus are urgently needed. In vitro models are a useful way to study SARS-CoV-2 biology in high throughput and simple systems. Currently, the golden standard to study in vitro SARS-CoV-2 infection is the monkey kidney cell line Vero E6, which is not directly translatable because of the difference in species and has been recorded to cause divergent evolution. This problem could be overcome with human immortalized cell lines or primary cell models, however, both cell lines and primary cell models show low permissiveness to infection. In this project and report, we optimized the infection ratios of immortalized cell lines by transducing them with SARS-CoV-2 receptor Ace2 and protease TMPRSS2. Transduction led to a higher permissiveness to infection as well as virus production, suggesting that these transduced immortalized cell lines can be used for further SARS-CoV-2 research as well as virus production for academic research purposes. In addition to the immortalized cell lines, we optimized the use of organoids and Air Liquid Interface (ALI) cultured cells derived from primary human airway cell samples for SARS-CoV-2 infection experiments. Furthermore, we showed that flow cytometry can be used to identify different cell populations within the ALI cultures using only the forward and side scatter. Taken together, the results show that there is a lot to be gained in translatability when it comes to in vitro models.

Table of contents

Abbreviations:.....	2
Abstract.....	3
Table of contents.....	4
1. Laymen’s summary	6
2. Introduction	7
2.1 Background.....	7
2.1.1 COVID-19.....	7
2.1.2 Transmission dynamics.....	7
2.1.4 Treatment strategies and vaccines.....	7
2.2 Coronaviridae	8
2.1.3 SARS and MERS.....	8
2.1.5 Origin.....	9
2.3.2 Translation of viral protein and genomic replication.....	12
2.3.3 Formation of the mature virion.....	12
2.3 In vitro cell models	12
2.3.1 Vero E6.....	13
2.3.2 Human cell lines.....	13
2.3.3 Human primary cultures.....	13
2.4 Aim of research	15
3. Materials and methods	16
3.1 Cell culture	16
3.1.1 Immortalized cell lines.....	16
3.1.2 Basal cells and air liquid interface (ALI) cultures: IN PROGRESS and CONFIDENTIAL.....	16
3.2 SARS-CoV-2 strains	16
3.3 Viral Infections	16
3.3 Confocal microscopy	17
3.4 q-RT PCR	17
3.5 Flow cytometry	17
3.6 Lentivirus production and lentiviral transduction	17
3.7 Western blot	18
3.8 Antibodies	18

4	Results	19
4.1	Improving SARS-CoV-2 infection rates in human cell lines	19
4.1.1	Vero E6 cells as a positive control to monitor SARS-CoV-2 infection.....	19
4.1.2	Infection with SARS-COV-2 in Vero E6 cells results in Golgi-dispersion...22	
4.1.3	Human immortalized cell lines present low SARS-CoV-2 infection rate...23	
4.1.4	Improving expression of SARS-CoV-2 receptors Ace2 and TMPRSS2 using lentiviral transduction.....	24
4.1.5	Ace2 and TMPRSS2 transduction can effectively increase SARS-COV-2 infection rates in A549 and Huh7 cells	26
4.2.1	Cell types in ALI cultures can be distinguished using flow cytometry	28
4.2.2	SARS-CoV-2 can infect Air liquid interface (ALI) cell culture	29
4.2.3	Using organoids for high-throughput compound screens.....	30
5	Discussion	32
6	Conclusion	36
7	Acknowledgments	37
8	Supplementary data	38
	References	40

1. Laymen's summary

SARS-CoV-2 is een virus dat sinds begin 2020 de wereld in zijn greep houdt. Vanaf het begin van de pandemie zijn er meer dan 4,5 miljoen doden gevallen en miljoenen mensen meer gehospitaliseerd. Daarnaast moet reguliere zorg worden uitgesteld en zucht de economie van vele landen onder de druk van lockdowns. Er zijn grote inspanningen gedaan voor de snelle ontwikkeling van medicijnen en vaccins. Een belangrijke stap in de ontwikkeling van elk medicijn of geneesmiddel is het testen van dit middel in het lab. Bij deze testen worden menselijke cellen gebruikt, die tientallen jaren geleden bijvoorbeeld uit een tumor zijn gehaald. Deze cellen zijn goed te vermenigvuldigen buiten het lichaam (in vitro), en kunnen wetenschappers inzicht geven in de reactie van menselijke cellen op een medicijn. Hoewel SARS-CoV-2 erg infectieus is in de context van de longen, is dit lang niet altijd het geval voor de cel lijnen. Het is echter wel essentieel voor het onderzoek om goed infecteerbare cellen te hebben. Als er te weinig infectie te zien is, kunnen namelijk ook geen verschillen worden gemeten tussen behandeling en controle. Om een cel lijn goed te kunnen infecteren moet de cel lijn de goede eiwitten aan de buitenkant laten zien. Belangrijke eiwitten voor SARS-CoV-2 zijn Ace2 en TMPRSS2. Deze eiwitten zorgen ervoor dat het virus zich kan hechten aan de cel en dat het zo geknipt wordt dat het de cel binnen kan treden. In het huidige onderzoek wordt vaak de "Vero E6" cel lijn gebruikt, omdat daarvan was laten zien dat die erg goed geïnfecteerd kan raken. De oorsprong van deze cel lijn is echter de aap, hierdoor kan de Vero E6 cel lijn ons minder zeggen over de reactie van menselijke cellen op infectie en mogelijke medicijnen. In dit verslag worden meerdere manieren beschreven om deze drempel te overkomen. De eerste manier is om de twee belangrijke eiwitten (Ace2 en TMPRSS2) in te brengen in de menselijke cel lijnen. Dit geeft het virus de gelegenheid om de cel lijn te kunnen infecteren. Een andere interessante mogelijkheid is het gebruik van primaire cel lijnen. Dit betekent dat er een monster wordt genomen van de luchtwegen van patiënten, bijvoorbeeld bij patiënten waar een ingreep in de luchtwegen moet worden uitgevoerd. Vervolgens wordt dat monster aan cellen van de patiënt verder gekweekt in het lab. De longen bestaan uit een heel scala aan cellen. Bij het nemen van een monster van de patiënt worden de long stamcellen gebruikt in het lab, deze kunnen zich nog ontwikkelen tot vrijwel alle cellen in een normaal long weefsel. Hierdoor kan dit scala aan cellen worden nagebootst in het lab. Dit maakt dit model dan ook een erg interessante optie om SARS-CoV-2 infectie in te bestuderen. In dit verslag worden beide modellen getest voor SARS-CoV-2 infectie.

2. Introduction

2.1 Background

In December 2019, a cluster of patients with symptoms of a contagious respiratory illness was determined in Wuhan, China¹. The infectious agent isolated from patients bronchoalveolar lavage fluid was determined to be a novel coronavirus; severe acute respiratory syndrome coronavirus 2 (SARS-CoV-2, called nCoV-19 at the time)^{2,3}.

2.1.1 COVID-19

SARS-CoV2 infection can lead to coronavirus disease 2019 (COVID-19). In 81 % of the cases, SARS-CoV-2 infection progresses with mild flu-like symptoms or even asymptomatic^{4,5}. Common symptoms are cough, fever and fatigue⁶. However, 14% of patients will develop severe respiratory illness and 5% is admitted to the Intensive Care Unit (ICU) with low oxygen saturation^{4,7}. COVID-19 disease becomes critical when patients develop acute respiratory distress syndrome (ARDS), respiratory failure, or multiple organ failure⁸. The case-fatality rate has been reported between 1-3%, depending on the country and severity of the outbreak⁹. Risk factors for developing severe COVID-19 disease include old age and co-morbidities, such as diabetes or cardiovascular disease^{10,5}. Additionally, a new phenomenon was observed where patients continue having infection-related symptoms (running out of breath, fatigue and loss of taste), long after the infectious particles have been cleared from the lungs¹¹. This phenomenon is called long COVID¹². On a population level, the virus presents a threat by overcrowding hospitals, which are not equipped to deal with an influx of patients of this scale. Examples of overcrowded hospitals were seen at the start of the pandemic in Italy, where health care systems collapsed. Regular hospital care has been scaled down in a majority of countries¹³. Since the initial outbreak in December 2019, the epidemic developed into a pandemic, affecting all continents and causing over 4,5 million deaths by September 2021¹⁴.

2.1.2 Transmission dynamics

In the past, authorities were able to contain the spread of other highly pathogenic coronaviruses like SARS and MERS, by employing effective isolation and quarantine measures after patients developed symptoms, resulting in a relatively limited outbreak¹⁵. One of the reasons this strategy did not work optimally with SARS-COV-2 is the relatively big proportion of patients with mild or no symptoms⁴. The lack of (severe) symptoms can interfere with effective diagnostics. It was estimated that infections from asymptomatic patients account for 24% of infections^{5,16}. Moreover, the timeframe between the start of infectious virus shedding and developing symptoms is longer^{17,18}. The contribution of infections originating from pre-symptomatic patients was estimated to be around 35%¹⁶. Another reason for the quicker spread of SARS-CoV-2 is the higher human-to-human transmission, as demonstrated by the higher reproduction number in a naïve population, R_0 (around 3.28)¹⁹.

2.1.4 Treatment strategies and vaccines

Finding prevention and treatment strategies for SARS-CoV-2 is imperative as the pandemic poses a great threat to global health, economy and stability. At the start of the pandemic, little was known about the treatment of infected patients and most therapies were focused on symptomatic treatments. As the pandemic progressed, more data were collected and different treatment strategies were tested or are still under review. Disease progression can be roughly divided into two stages; the first stage, where most symptoms are caused by replication of the virus and the second stage, where symptoms are caused by the disproportionate response of the immune system. The first stage can be

treated with monoclonal antibodies and antivirals. Currently, the only medicine approved by the European medicines agency (EMA) and the food drug administration (FDA) is Remdesivir^{20,21}. Remdesivir is an adenosine nucleotide analog pro-drug that is recommended to hospitalized COVID-19 patients²². Additionally, monoclonal antibody treatments such as Casirivimab, Imdevimab and Sotrovimab are under rolling review or have been granted emergency use authorization²³. Generally, monoclonal antibody treatments are recommended to early-stage COVID-19 patients who are at risk of clinical progression²⁴. The symptoms in the second stage of COVID-19 can be managed with glucocorticoids such as dexamethasone²⁵. The use of these glucocorticoids is recommended in hospitalized patients in need of supplemental oxygen. Additionally, antibiotics can be given to treat bacterial co-infections. Next to the currently recommended treatments, there are proposals for other COVID-19 treatments such as soluble Ace2²⁶. Despite great efforts to find the best treatment plan for COVID-19, to date, there is no treatment effective enough to prevent a large influx of patients in hospitals and ICUs. That is why testing new treatment options remains crucial.

In addition to treatment strategies, efforts have been made since the beginning of the pandemic to find a vaccine for disease prevention. A combination of increased funds by governments buying the vaccine before its development and previous research for an Ebola and SARS vaccine led to the rapid development of several highly effective SARS-CoV-2 vaccines²⁷. The Spike protein on the outside of the virus is an essential target for the immune response, and therefore vaccine development²⁸. Currently, several vaccines with different mechanisms are approved by the EMA and the food FDA. The most commonly used vaccine platforms are mRNA vaccines (Pfizer, Moderna) and vector vaccines (Janssen, Astra-Zeneca). In addition, there are more than 50 other vaccines in development including whole inactivated, attenuated and subunit vaccines²⁸.

The approved vaccines all target the spike protein, which could lead to (partial) resistance of new virus variants to the immune response elicited by the vaccines. Indeed, in the course of the pandemic, new virus variants emerged that gained a foothold over time, starting with the Alpha variant (B.1.1.7), continuing with the Beta (B.1.351) and Gamma (P.1) variants, then the Delta variant (B.1.617.2)²⁹. The variants get the upper hand over other variants either because they have stronger binding to the entry receptor, or they can evade neutralizing antibodies against spike. The combination between the rise of new variants that can spread through a vaccinated population and the fact that far from the whole world population has been vaccinated because of vaccine inequity and hesitancy, means that research directed towards understanding more of SARS-CoV-2 biology continues to be highly valuable.

2.2 Coronaviridae

SARS CoV-2 is a member of the *coronaviridae* family, which consists of several different viruses¹. Common characteristics of viruses in the *coronaviridae* family are the large single-stranded, positive-sense RNA genome and the envelope with spike proteins resembling a crown-like structure to which the family owes its name³⁰. Within the *coronaviridae* family, SARS-CoV-2 belongs to the lineage of Beta-coronaviruses 2B^{8,31}. This grouping is based on the difference in size and sequence of the nsp1 non-structural protein³².

2.1.3 SARS and MERS

The majority of coronaviruses are limited to an animal reservoir, such as Infectious Bronchitis Virus (IBV), Bovine Coronavirus (BCoV), Murine Hepatitis Virus (MHV) and Feline Coronavirus (FCoV)³³. However, there are seven coronaviruses known to be able to infect humans, ranging from common cold viruses (HCoV-229E, HCoV-NL63)³⁴ to viruses causing severe respiratory disease (SARS, MERS)^{35,36}. Currently, there are three highly pathogenic coronaviruses known to cause severe respiratory illness in humans; Severe Acute Respiratory Syndrome (SARS), Middle East Respiratory Syndrome (MERS) and SARS-CoV-2. The first SARS outbreak originated in 2002 in Guangdong province, China, where the

zoonotic introduction of SARS from bats to humans was likely catalyzed by spill-over events at several wild-animal food markets^{2,37}. MERS coronavirus appeared for the first time in 2012 in Saudi Arabia and was caused by a zoonotic transmission from dromedary to human³⁸.

2.1.5 Origin

Similar to SARS and MERS, the outbreak of SARS-CoV-2 was likely the result of a zoonotic event. The original host of SARS-CoV-2 is the bat, as is the case for most beta-coronaviruses^{39,40}. The probable origin of SARS-CoV-2 in bats was demonstrated by a 96% resemblance of SARS-CoV-2 to the RaTG13 coronavirus found in *Rhinopholus Affinis* bats³⁹. The intermediate host that made the jump to human transmission possible is still under debate. The initial hypothesis was that Pangolins were the intermediate host because several domesticated Pangolins were found to carry SARS-CoV-2. However, this hypothesis was disproved by the finding of a unique RRAR motif in the spike protein^{41,42}. A plausible location for the zoonosis event is the Huanan Seafood Wholesale Market, where most of the first patients had a connection, either by working or visiting the market⁴³. Nonetheless, some researchers are critical about the Huanan Seafood Market being the zoonotic location, saying it was only a catalyzer because not all first infections could be traced back to the market⁸.

2.3 Virus structure and replication

The genomes of *coronaviridae* encode for non-structural proteins nsp1-16 at the 5' end³⁰. Additionally, coronaviruses have several structural proteins in common, encoded on the open reading frames (ORF) at the 3' end of the genome; a surface glycoprotein (S), an envelope protein (E), a membrane glycoprotein (M) and a nucleocapsid protein (N)(figure 1)⁴⁴. The replication cycle of SARS-CoV-2 is still under investigation, however, the steps to successful infection are expected to resemble that of other coronavirus infections (figure 2). The next paragraphs will describe the different stages of SARS-CoV-2 infection in more detail.

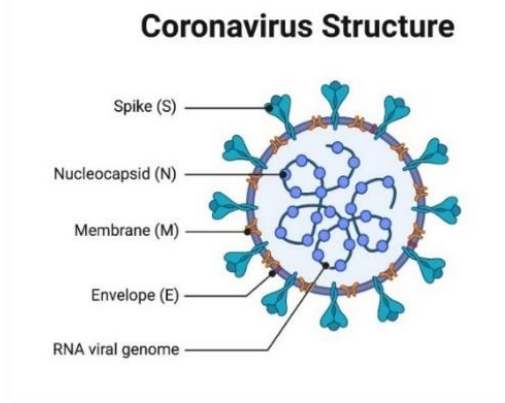


Figure 1: Coronavirus structural proteins. Spike (S), Nucleocapsid (N), Membrane (M), Envelope (E), RNA viral genome. Adapted from 'King J 'Kosinski-CM 'Sundberg, E. *Coronavirus Structure, Vaccine and Therapy Development. Biophysical society. 2020.*

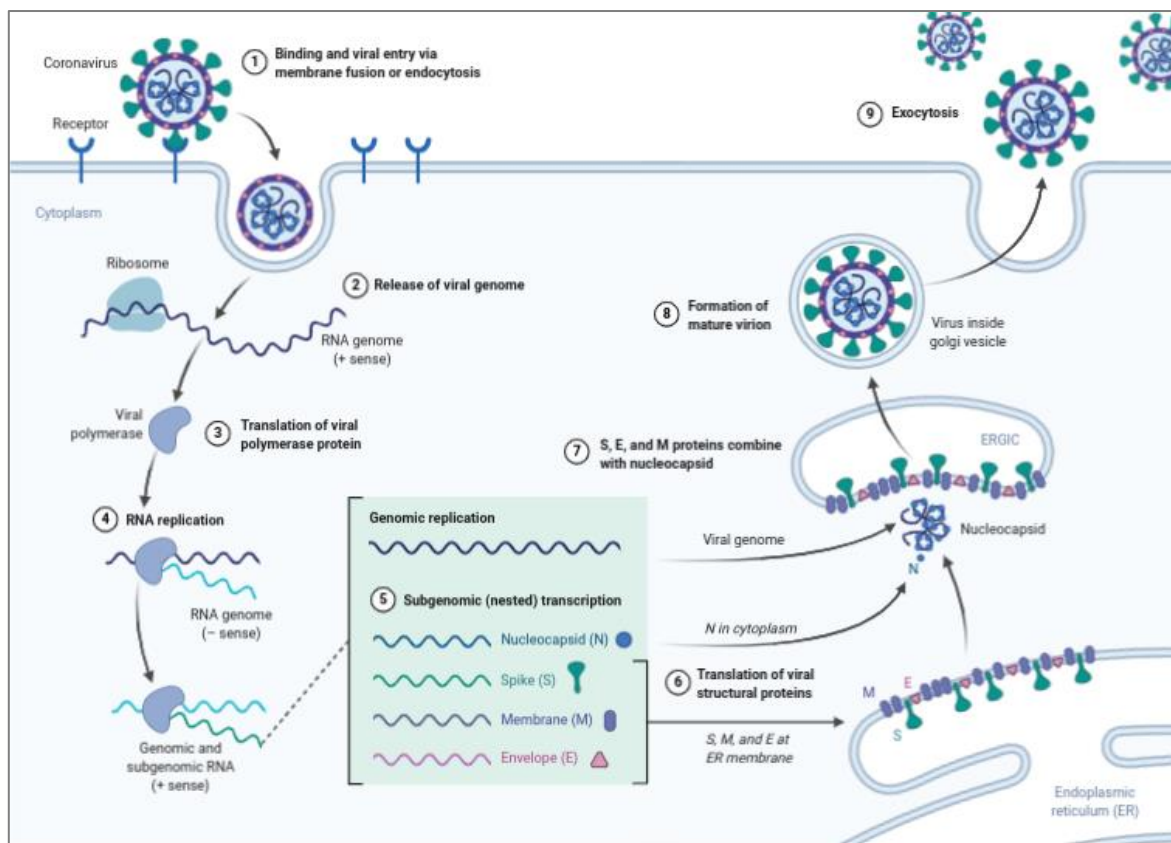


Figure 2: Coronavirus replication cycle. The virus enters the cells through binding a receptor on the host-cell surface (1). The virus is taken up by endocytosis and the viral lipid envelope fuses with the endosomal membrane. After entry, the viral genome is released into the cytosol (2). This viral genome is positive-stranded RNA, and can therefore be directly translated (3). Translation of the viral polymerase takes place, and the viral RNA-dependent-RNA-polymerase starts replicating the viral genome (4). In addition to the complete genome replication, subgenomic RNAs are produced that encode for structural proteins N, S, M and E (5, 6). A new viral particle is produced inside an ERGIC vesicle (7) and transported to the plasma membrane (8), where the virion is released through exocytosis (9). *Adapted from 'King J 'Kosinski-CM 'Sundberg, E. Coronavirus Structure, Vaccine and Therapy Development. Biophysical society. 2020.*

2.3.1 Binding and viral entry

SARS-CoV-2 enters the host cell using the Spike protein (S) that is embedded in the viral lipid envelope (figure 1). The spike protein consists of two subunits. The S1 subunit is exposed to the surface and can bind to the receptor through a receptor-binding domain (RBD)(figure 3)⁴⁵. Similar to SARS-CoV and other respiratory viruses, SARS-CoV-2 uses Angiotensin Converting Enzyme 2 (ACE2) as an entry receptor^{46,39}. Although the RBD from SARS-CoV and SARS-CoV-2 have a close resemblance, it has been suggested that subtle key residue changes in SARS-CoV-2 S improve Ace2 receptor binding⁴⁷, which contributes to higher infectivity⁴⁸.

The second subunit in the spike protein is the highly conserved S2 subunit. This subunit contains the transmembrane domain that anchors the S protein in the viral lipid envelope (figure 3). In addition, the S2 subunit contains a fusion peptide and two heptat repeats (HR) responsible for membrane fusion⁸. In contrast with SARS-CoV, the SARS-Cov-2 spike protein is reported to have a high membrane-fusion potential⁴⁹, this hypothesis was strengthened by the observation of syncytia after SARS-CoV-2 infection, which are rarely observed with SARS-CoV infection⁵⁰. Moreover, a difference of 8 residues was found between SARS-CoV-2 HR1 and SARS-CoV HR1. These residues were predicted to contribute to enhanced interaction between the HR1 and HR2 domains⁵⁰. This might suggest a possibility for the virus to directly enter the cell at the cell membrane instead of in the endosomes. The enhanced membrane fusion potential may provide a second reason for higher SARS-CoV-2 infectivity.

A condition for membrane fusion is cleavage, also referred to as ‘priming’ of the S protein by host proteases. Cleavage contributes to conformational changes, that allow the S protein to start fusion of the lipid envelope with the host membrane. There are two cleavage sites present in the SARS-CoV-2 S-protein: the first between S1 and S2 (S1/S2) and a second cleavage site within S2 (S2’).

The proteases Cathepsin L, B and transmembrane protease/serine subfamily member 2 (TMPRSS2) have all been described to cleave the S protein from other coronaviruses^{51,52}. Indeed, experiments with TMPRSS2 inhibitor camostat mesylate show that TMPRSS2 inhibition can partly block SARS-CoV-2 virus entry⁵³. When treated with a combination of camostat mesylate and E-64d, a compound that blocks Cathepsin B/L activity by elevating the endosomal pH, viral entry was completely abrogated⁵³. This could suggest that endosomal Cathepsin B/L can play a role in viral entry under certain circumstances. Contrarily, dr. Böttcher-Friebertshäuser and colleagues showed that treating Calu-3 cells with Cathepsin inhibitor E-64d had no protective effect against infection, whereas treating with TMPRSS2 inhibitors did⁵⁴. Additionally, Poehlmann et al. found that TMPRSS2 expression in E-64-treated cells effectively rescued viral infection. Taken together, the results indicate that although Cathepsin B/L can contribute to infection in the absence of other proteases, TMPRSS2 is the most important protease for S priming⁵³.

A distinction between the SARS-CoV-2 S and SARS-CoV S, is a new polybasic cleavage site (RRAR) in the S1/S2 cleavage site^{55,45}, giving the virus the advantage to be cleaved by highly expressed

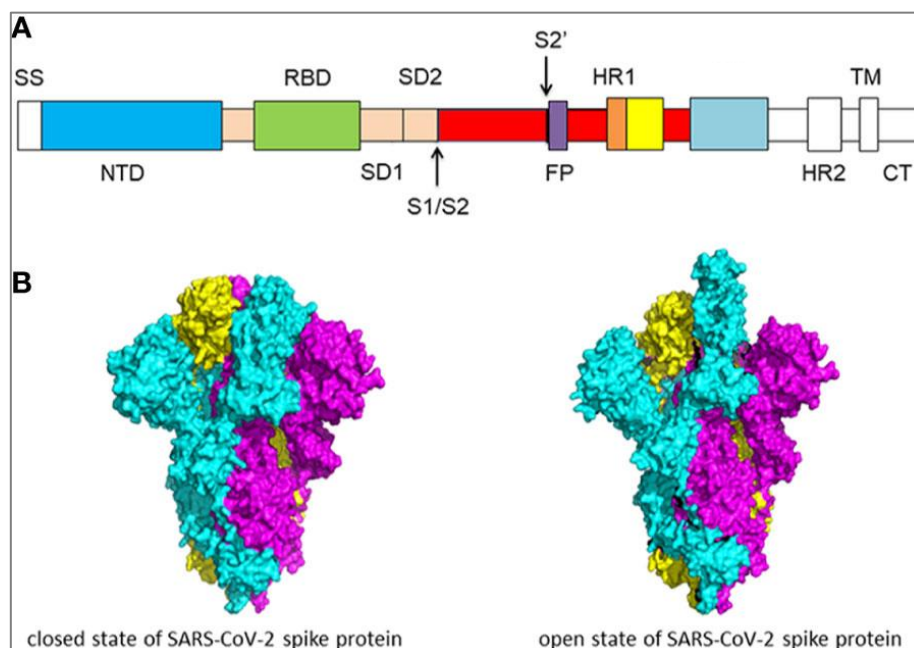


Figure 3: SARS-CoV-2 spike protein structure. A) primary structure of the SARS-CoV-2 spike protein divided in two subdomains SD1 and SD2, contain different domains: N-terminal domain (NTD), Receptor binding domain (RBD), Transmembrane domain (TM) and Cytoplasmic tail (CT). After cleavage at the two cleavage sites S1/S2 and S2’, the fusion peptide (FP) and two heptat repeat domains (HR) are responsible for membrane fusion. B) Conformational changes after cleavage and subsequent activation of the spike protein. *Adapted from SARS-CoV-2: Structure, Biology, and Structure-Based Therapeutics Development, Mei-Yue Wang, Rong Zhao, Li-Juan Gao, Xue-Fei Gao, De-Ping Wang and Ji-Min Cao*

host protease furin^{54,4}. This cleavage site has not been previously described in SARS-CoV-related betacoronaviruses, but has been described in HK1 and MERS⁵⁶. Moreover, a similar furin-like cleavage site was suspected to be an important virulence factor for the highly pathogenic H5N1 influenza strain⁵⁷. It was shown with a Murine leukemia virus pseudotyping system containing SARS-CoV-2 S or SARS-CoV S, that as a result of the furin-like cleavage site, SARS-CoV-2 S could be cleaved during biosynthesis of new viral particles⁴⁵. Both furin and TMPRSS2 are highly expressed in the lung epithelium, further strengthening the hypothesis that both play an important role in infection^{58,59}.

2.3.2 Translation of viral protein and genomic replication

After the viral membrane has fused with the cellular membrane, the viral genome will be released into the cytoplasm of the cell. The viral genome is positive sense and can therefore be translated directly. SARS-CoV-2 contains several ORFs of which the largest two are located at the 5' end of the viral genome. These two ORFs (ORF1a/b) translate for two polyproteins. ORF1a and b overlap at the 5' end, however, ORF1b is longer. This is caused by a -1 frameshift causing the ribosome to skip over the stop codon of ORF1a⁶⁰. The polyproteins are cleaved into 16 functional non-structural proteins (NSPs) by viral proteases Main protease (Mpro) and Papain-like protease (PLpro), also referred to as NSP5 and 3, respectively⁶¹. In addition to the 16 NSPs encoded on the first two ORFs, the SARS-CoV-2 genome contains more ORFs encoding for the four structural proteins; Spike (S), Envelope (E), Nucleocapsid (N) and Matrix (M) proteins as well as more non-structural proteins involved in, amongst others, immune evasion⁶¹. One of the proteins that can be formed after cleavage of polyprotein 1a/b, can form the RNA-dependent RNA polymerase (RDRP). Subsequently, the RDRP will start with replication of the genome. During this replication, several subgenomic RNA species can be generated using the negative-sense replication intermediates⁶¹. It has been reported that genome replication of SARS-CoV-2 happens in double-membrane vesicles, a process controlled by viral NSPs⁶². However, there needs to be more research on this mechanism in a SARS-CoV-2 specific situation, as these conclusions are mostly drawn from homology to other coronaviruses.

2.3.3 Formation of the mature virion

After the structural proteins M, E and S have been translated, they have an ER retention signal, which causes the proteins to localize to the ER membrane. The Nucleocapsid protein (N) binds the viral RNA. In this binding only the full-length positive-sense RNA is bound⁶². Subsequently, the nucleocapsid protein will bind the M protein that is embedded in the ER or ERGIC membrane, to further condensate the viral RNA and start with the formation of the viral particle. A hypothesis about the mechanism behind this RNA condensation is a phenomenon called Liquid-liquid phase separation and is likely triggered by packaging sequences in the SARS-CoV-2 genome⁶³. After all the structural proteins and the full-length genome are recruited, the virion will form completely and bud off from the ERGIC, to be directed towards the cell membrane where a new virus particle is released.

2.3 In vitro cell models

Investigating SARS-CoV-2 mechanisms and anti-viral compounds in vitro is an indispensable step to developing treatment strategies or vaccines on animal models or in clinical trials. From the start of culturing the first in vitro cell line HeLa, there have been fast developments in the field of in vitro models⁶⁴. An extensive array of different cell lines have been isolated and immortalized⁶⁵. 2D cell lines can be cultured as either an adhesive cell line or cell lines in suspension, depending on their properties. They have been fundamental for previous research in cell physiology, metabolism and kinetics⁶⁴. Likewise, much of SARS-CoV-2 research has been performed on immortalized cell lines³⁹. Most frequently used cell lines included: Vero E6 (green African monkey kidney), Huh7 (human hepatocyte carcinoma) Caco-2 (human colon adenocarcinoma), Calu-3 (human non-small cell lung cancer) and HEK293T (human embryonic kidney cells)⁶⁶. Each of the cell lines has its advantages and drawbacks.

2.3.1 Vero E6

The Vero E6 African monkey kidney cell line has been essential in SARS-CoV-2 research predominantly because of its ability to produce high titers of SARS-CoV-2 virus after infection^{67,68}. It was determined previously that this cell line lacks a type I IFN response due to a 9 Mb deletion in chromosome 12^{69,70}. Additionally, the cell line has been reported to highly express SARS-CoV-2 entry receptor Ace2^{71,66}. Both factors can contribute to the ability of the cell line to produce high virus titers⁷². These properties contributed to the fact that the Vero E6 cell line is frequently used to produce virus stocks for academic research.

Recently it was found that virus production by Vero E6 drives a different virus evolution^{73,74}. Vero E6 cells are speculated to favor SARS-CoV-2 with Spike protein lacking the furin-like cleavage site at S1/S2, by providing lower selective pressure than human tissues would. Virus produced in Vero E6 cells often contained a deletion abrogating the S1/S2 furin-cleavage site⁷² as well as another S1/S2 cleavage site that the virus has in common with SARS-CoV⁷⁴. Although the virus can still proliferate in Vero E6 cells, mutations around the S1/S2 furin-like cleavage site were reported to significantly impact virus fitness in human cell lines and animal models^{45,73}. This is an important drawback and could lead to unnoticed differences between the virus strains used in research and virus strains circulating amongst the population, with as a result inaccurate findings in SARS-CoV-2 research.

2.3.2 Human cell lines

Human cell lines used in SARS-CoV-2 research are Huh7, Caco-2, Calu-3 and HEK293T. The fact that they originate from human tissue improves the translatability of SARS-CoV-2 research in these cell lines. A complication with these cell lines is their poor permissiveness to SARS-CoV-2 infection. Attempts have been made to make a virus that is adapted to the Huh7 cell line, by passaging the virus in this cell line until the virus titer goes up⁷⁵. However, this strategy provides the same disadvantages as passaging SARS-CoV-2 in Vero E6 cells, as it will not optimally reflect the virus circulating in the population. This is demonstrated by the lower Ace2-dependence of SARS-CoV-2 infection with the adapted viral variant⁷⁵. A different alternative to increase virus-permissiveness in human cell lines is to improve their expression of SARS-CoV-2 priming protease TMPRSS2, a strategy that was shown to significantly increase viral production in Vero E6 cells⁶⁷.

2.3.3 Human primary cultures

Another frequently used technique to represent lung tissue in vitro is the Air Liquid Interface (ALI) filter on which to grow and differentiate primary human basal cells. These basal cells have been harvested from patients undergoing bronchoscopy (figure 5). The basal cells are grown in the appropriate growth media until sufficient amounts to seed on an ALI filter are obtained (methods). Subsequently, the basal cells are seeded on an ALI filter and provided with growth media to trigger differentiation. After a few weeks, the cells on the ALI filter have differentiated into four different cell types; Mucin-producing goblet cells, Ciliated cells, Basal cells and Club cells (figure 4)⁷⁶. Air Liquid Interface cell cultures either of primary human nasal epithelial cells (HNEC) or lung cell lines have been used in the past to model different cellular diseases, for example cystic fibrosis⁷⁷. In addition, they have been used for research about air-borne pathogens as well as environmental triggers of the airways such as smoking⁷⁸. Because these ALI filters mimic the situation in the lung with fluid on the basal side and air on the apical side, these models are considered to have a closer resemblance to the in vivo situation.

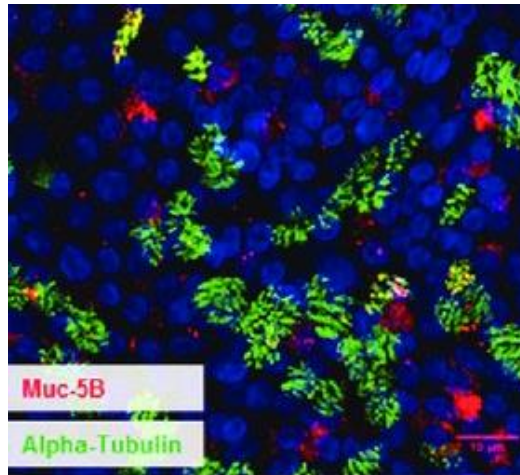


Figure 4: Cell types in HNEC cultures on Air Liquid Interface (ALI) filters. Cells are stained for Muc-5B (red, Mucin-producing goblet cells) and Alpha-Tubulin (green, Ciliated cells). Nuclei are marked with DAPI (blue) Adapted from LaRanger R et al., Tissue Engineering, 2017

ALI cell culture can provide a useful model to study the different cell types in infection, however, it is still a 2D model, which means that the 3D structure of the lung epithelium is not represented in these models. If an experiment requires a 3D structure in an in vitro situation, an important model would be the organoids. When defining organoids as a 3D structure grown from stem cells that are differentiated, the first organoids were described in 2012⁷⁹. The conventional way of generating organoids is by directly taking either pluripotent embryonic stem cells or induced pluripotent stem cells and adding them to a matrix⁷⁹. However, they can also be generated from the Air liquid interface (ALI) cell cultures. Beekman and colleagues developed a technique to cultivate human airway organoids from differentiated cultures grown on Air Liquid Interface filters (methods). To generate the organoids, the differentiated cell layers are detached from the ALI filter and transferred to a gel matrix. The existence of “loose ends” in the cell layers will trigger fusion of the edges and thereby the formation of organoids. This step can result in conventional organoids, that contain cilia on the inside, as well as “inside out” organoids, where the cilia are situated on the outside and the cell polarity is completely reversed (figure 5). This model provides several advantages; organoids contain different cell types of the lung epithelium and they mimic the 3D situation. Additionally, organoids can be used for high-throughput screening, because from one ALI filter an array of organoids can be generated, making it possible to test more than one condition.

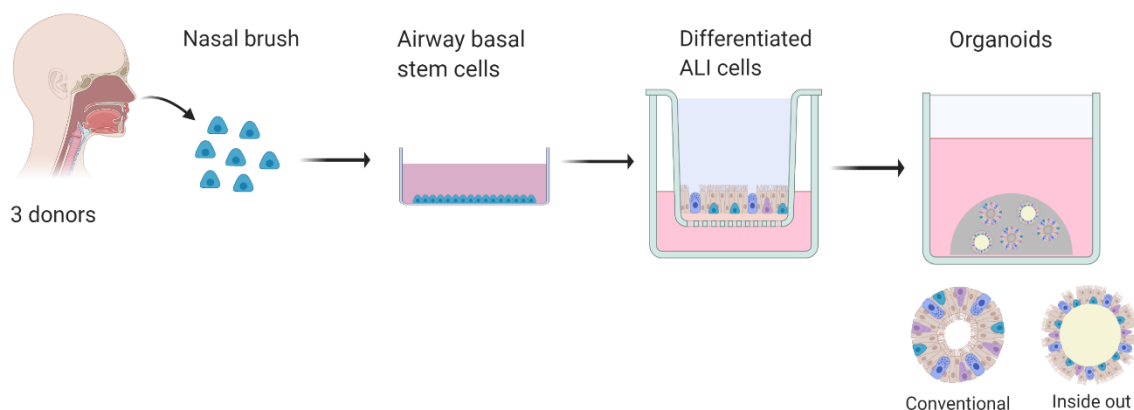


Figure 5: Cell culture primary cells to Air Liquid interface (ALI) filters and/or organoids. Basal cells are harvested using a nasal brush, the basal stem cells are grown until sufficient amounts are reached to seed the basal stem cells on ALI filters. On the ALI filter, the airway basal stem cells differentiate. To generate organoids, the cell layers are detached from the ALI filters and added to matrix droplets, where they form conventional and inside out organoids. Made in Biorender.

2.4 Aim of research

SARS-COV-2 is one of the biggest global health threats in over a century. Despite the rapid development of several different vaccines, the pandemic is not under control in a large part of the world. The threats of new vaccine-resistant variants developing or the re-introduction of another coronavirus through a separate zoonotic event are continuous. Thus there is still a great need for more information about the mechanisms behind SARS-COV-2 infection, replication and transmission. To investigate these mechanisms and possible compounds working against SARS-CoV-2 and other coronaviruses, good in vitro cell culture models are the first step.

Currently, most in vitro SARS-CoV-2 research is performed on monkey kidney Vero E6 cells or with a high MOI in immortalized lung carcinoma cells (Caco-2 or Calu-3), because they harbor capacity for infection⁶⁶. However, these cells differ from in vivo human tissue in a number of aspects. They do not represent the diversity of cells in the lung tissue. Additionally, Vero E6 cells drive the evolution of the virus that could lead to a virus that is less infectious in humans and is therefore not a good model system.

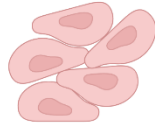

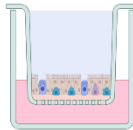
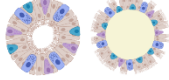




Cell model	1. Vero E6 cells 	2. Transduced human cell lines 	3. Air Liquid Interface (ALI) cells 	4. Organoids 
Origin	 Monkey	 Immortalized cell line	 Primary cells	 Primary cells

Figure 6: Alternative in vitro cell models for SARS-CoV-2 infection. 1. Vero E6 cells; Rhesus monkey kidney cells, 2. Human immortalized cell lines that can be transduced for higher infection. 3. Air Liquid Interface cells derived from primary cells and 4. Organoids, derived from the ALI cells. Made in Biorender.

To find a suitable model, three characteristics have to be taken into account. The first characteristic is the origin of the cell line; although Vero E6 cells have been instrumental for SARS-CoV-2 and other virus research, these cells are derived from African monkey kidney tissue and therefore do not contain the human genome. Other characteristics of an improved model comprise the functional heterogeneity, polarity and 3D characteristics of lung cells^{80,81,64}. The cell lines currently used in research do not represent the different cell types present in lung tissue. The last characteristic defined for a better model is permissiveness to infection. In order to test the influences of different compounds on infection, the virus infection in vitro needs to be in a range where significant change can be detected.

In addition to the importance of having translatable cell model systems for the host, the properties and prevalence of the virus strains used in research should match the strains circulating in the general population. Moreover, multiplying the virus for research purposes could lead to differences between the virus that is circulating in the population and the virus used in the lab, with as a result inaccurate findings. The problem of a divergent virus evolution was recently reported with the use of Vero E6 to amplify the virus⁷³. Hence, it is essential to find better in vitro models that reflect the human in vivo characteristics and do not drive divergent virus evolution.

This project and thesis have the aim of finding more efficient and translatable in vitro cell culture models for SARS-CoV-2 infection and virus production for academic research. These cell culture models comprise human immortalized cell lines Huh7 and A549 transduced with the two SARS-CoV-2 entry proteins; Ace2 and TMPRSS2. In addition, primary airway cell cultures and lung organoids are tested for their potential in SARS-CoV-2 research. Ultimately, finding more translatable models for SARS-CoV-2 infection can contribute to more accurate SARS-CoV-2 research, with as a consequence better understanding of SARS-CoV-2 biology and possibly new insights into treatment options.

3. Materials and methods

3.1 Cell culture

3.1.1 Immortalized cell lines

Vero E6 WT, Huh7 WT, Huh7+Ace2-GFP, Huh7+Ace2-GFP+TMPRSS2, MRC5 WT, Caco2, A549 WT, A549+Ace2-GFP+TMPRSS2 cell lines were cultured in Dulbecco's modified Eagle's medium (DMEM) 1x Glutamax™ (Gibco, +4.5 g/L D-Glucose + Pyruvate) supplemented with 5% fetal bovine serum (FBS, Thermo Scientific), 100 U/mL penicillin, 100 µg/mL streptomycin and 2mM L-Glutamine. Calu3 cells were grown in F12/DMEM supplemented with 10% fetal bovine serum (FBS, Thermo scientific), 100 U/mL penicillin, 100 µg/mL streptomycin and 2mM L-Glutamine. HK1 and MelJuSo were cultured in RPMI 1640 medium supplemented with 5% fetal bovine serum (FBS, Thermo scientific), 100 U/mL penicillin, 100 µg/mL streptomycin and 2mM L-Glutamine. All cell lines were grown at 37 °C and 5% CO₂ and obtained from ATCC (American Type Culture Collection). The Vero E6, Huh7, Caco2, Calu3, A549, HK1, MelJuSo and MRC5 cell lines were obtained from ATCC (American Type Culture Collection).

3.1.2 Basal cells and air liquid interface (ALI) cultures: **CONFIDENTIAL**

3.2 SARS-CoV-2 strains

Three different SARS-CoV-2 strains were used in this project. The first strain is the NL2020 strain. This strain is commonly accepted to be the most prevalent strain in the Netherlands during the beginning of 2020. The strain was obtained from the European virus archive global (EVAg). The second strain, patient1 (Pat1p3), was obtained from a patient sample in the Universitair Medisch Centrum Utrecht (UMCU). A third virus strain containing a green fluorescent protein (GFP) insert was generated and kindly provided by Dr. Volker Thiel from the University of Bern, Institute of Virology and Immunology (Genbank MN996528.1). This strain will be referred to as the GFP strain from here on. The strains were multiplied in Vero E6 cells. Virus titers of all three strains were determined by infecting Vero E6 cells(?) in a 96-well plate with different dilutions of the virus sample. The 96-well plates were visually screened for cytopathic effect (CPE). The tissue culture infectious dose (TCID₅₀) was determined by finding the dilution that caused CPE in 50% of the wells. This TCID₅₀ could be used to determine the virus titer.

3.3 Viral Infections

Cells were seeded one day prior to infection in their respective complete medium with 2% Fetal Calve Serum (FCS). The cells were seeded on 12 well cell culture treated plates directly, or on 18 mm coverslips. On coverslips, 50.000 cells were seeded. On 12-well culture plates the seeded cell amount ranged from 50.000 to 250.000, depending on the cell line and experiment. All infections with the

SARS-CoV-2 NL2020, -Patient1 or -GFP strain were performed under Bio Safety Level 3 conditions (BSL3) by Patrique Praest. Cells were infected with a multiplicity of infection (MOI) of 0.1, 0.05 or 0.01 virus particles per cell. To infect the cells, the virus was added to the wells in the appropriate medium for that cell line with 2% FCS. When infecting primary cells on ALI culture filters, the virus was added to the apical side. Before taking infected samples out of the BSL3 lab for qPCR, confocal imaging or flow cytometry, the virus was inactivated by heating the samples for 30 min at 75 C or adding 4% formaldehyde for 20 min with or without glutaraldehyde, respectively.

3.3 Confocal microscopy

For the confocal microscopy, cells were seeded on 18 mm thick glass coverslips and infected with the different SARS-CoV-2 strains. Coverslips or ALI filters were fixed with 4% PFA for at least 20 minutes and transferred to clean containers before taking them out of the BSL3 lab. Harvesting was done at different time points post-infection (8 hours, 24 hours, 48 hours). The fixed coverslips or ALI filters were stained with antibodies (listed in “3.8 Antibodies”). The coverslips were analyzed using a Zeiss LSM880 Fast Airyscan Microscope with 405 nm, 561 nm and argon multiline lasers, an internal Zeiss spectral 3 PMT detector and spectroscopic detection using a Plan-Apochromat 63x/1.2 glycerol objective with the guidance of Dr. Wilco Nijenhuis from the group of Prof. Dr. Lukas Kapitein. Z-stacks were created and images were analyzed with FIJI (Fiji Is Just ImageJ).

3.4 q-RT PCR

For qPCR analysis, cell lines were infected with three different SARS-CoV-2 strains (GFP, NL2020 and Patient1). A cell sample was taken and dissolved in Trizol (Thermofisher) or the supernatant was measured. The supernatant was heat-inactivated (30 min, 75°C) and the samples were taken out of the BSL3 lab. From the cell samples, RNA isolation was performed using an RNA isolation kit (Norgen Biotek Corp). Then, viral RNA was detected; a 10 µL reaction contained 1 µL Viral RNA sample, 2,5 µL 4*TaqMan fast Virus 1-Step Master Mix (Applied Biosystems, Thermo Fisher Scientific), 0,5 µL E-gene primer-probe mix (ACAGGTACGTTAATAGTTAATAGCGT (Forward), ATATTGCAGCAGTACGCACACA (Reverse)) and 6 µL H₂O. The samples were analyzed in the StepOnePlus™ Real-Time PCR (Thermofisher, catalog number 4376600) measuring VIC. Thermal cycling was performed for 10 min at 55°C, 3 min at 95°C, then 45 cycles of 15 sec 95°C, 30 sec 58°C.

3.5 Flow cytometry

Cells were seeded 24 hours prior to infection in their respective medium with 2% FCS. The cells were harvested with TrypLE to preserve surface proteins. Harvesting and fixation of the cells happened at 8, 24 or 48 hours, depending on the experimental setup. The cells were centrifuged at 400 G, the supernatant was removed and the cells were resuspended in ice-cold PBA buffer (phosphate-buffered saline (PBS), 0.5 % bovine serum albumin and 0.02% Sodium Azide). When staining intracellular proteins, a buffer solution of PBS, 0.5% saponin and 2% cold FCS was added before staining to permeabilize the cells. To determine Spike, Ace2 or TMPRSS2 expression in virus-infected cells, the cells were incubated with primary antibodies. After a 30 minutes incubation at 4°C, cells were washed with cold PBA buffer and incubated with the secondary antibody. The secondary antibody was incubated for 30 minutes (dark, 4°C) and the residual antibody was removed with PBA. The protein expression was detected using the FACS Canto II (BD Biosciences) and the data were analyzed using FlowJo V10 software.

3.6 Lentivirus production and lentiviral transduction

Cell lines were transduced using lentiviral delivery systems. Lentivirus was produced through transfection of 62.500 HEK293T cells. 1,5 µL of Mirus LTI was added to 50 µL of serum-free medium (Opti-MEM) and incubated for 5 minutes. 375 µL plasmid was mixed with the serum-free medium and Mirus (lentiviral packaging mix and the plasmid with the DNA of the desired protein (ACE2 or TMPRSS2)). After 20 minutes of incubation, the mix was added on top of the HEK293T cells. After 3 days, supernatant from virus-producing cells was frozen in or filtered to inactivate any residual lentivirus-producing HEK293T cells. The lentivirus was used to transduce wildtype cells in presence of 8 µg/mL polybrene. The plate was centrifuged for 90 minutes at 2000 RPM (877 G) and 33 °C. Cells containing the ACE2-GFP and/or TMPRSS2 construct were selected by blasticidin resistance (10 µg/mL) for 10 days. Pseudotyped virus was produced and used in the BSL2 lab according to the methods described by Bloom et al⁸².

3.7 Western blot

5 million cells were counted per cell line to isolate the protein sample from. The cells were lysed using 1% Triton lysis buffer (150 mM NaCl + 50 mM Tris pH 7.5 + 1% Triton X-100) with added protease inhibitors AEBSF (1:1000) and Leupeptin (1:1000). The sample was centrifuged for 15 minutes (14000 rpm, 4°C) and the supernatant was diluted in DTT buffer. Subsequently, the sample was boiled for 5 minutes at 95°C. Proteins were separated using SDS-PAGE with a Bolt 4-12% Bis-Tris Plus gel (Invitrogen, NW04125) and transferred to a PVDF membrane for 10 minutes, 25V with a Trans-Blot Turbo transfer system (Biorad). The membranes were blocked for 1 hour in block buffer (PBS Tween + 4% ELK) and incubated overnight (4°C) with primary antibodies diluted in PBS Tween + 1% ELK. Membranes were washed and incubated in the dark with secondary antibodies labeled with Horse Radish Peroxidase (HRP) for 1 hour at room temperature or 2 hours cold. After washing the membranes with PBS Tween + 1% ELK, Pierce ECL Western Blotting Substrate (Thermo Scientific) was added to the membranes and the proteins were detected using the Image Quant LAS 4000.

3.8 Antibodies

For the Western blot, the following primary and secondary antibodies were used: rabbit-anti-Histone (1:5000, Cell Signaling Tech #9715), mouse-anti-Actin (1:10.000, Millipore #MAB1501R), mouse-anti-Rabbit (HRP, 1:10.000, Jackson #211-032-171) and goat-anti-mouse (HRP, 1:10.000, Jackson #115-035-174), mouse-anti-Ace2 (1:500, antibodies-online), rabbit-anti-TMPRSS2 (1:500, Fisher Thermo Scientific). For Flow cytometry, the following antibodies were used; goat anti-human IgM+ IgG (H+L) (1:160, Jackson #109-116-127), human anti-SARS-CoV-2 Spike (1: 682, REGN #10987), mouse-anti-Ace2 (1:90, antibodies-online), goat-anti-mouse PE (1:500, Dako #R0480), rabbit-anti-TMRPSS2 (1:15, Fisher Thermo scientific) and goat-anti-rabbit PE (1:1000, Southern biotechnology #4050-09). For confocal imaging, the following antibodies from the group of Lukas Kapitein were used; rabbit anti-SARS-CoV-2 Spike S1 (Sino Biological, #40150-R007), mouse anti-dsRNA (J2, Sci Cons, #10010200), DAPI (Sigma-Aldrich), Atto 647N Phalloidin (ATTO-TEC), mouse anti-GM130 (BD Biosciences, #610823) antibodies.

Results

3.2 Improving SARS-CoV-2 infection rates in human cell lines

The models used in current SARS-CoV-2 research are not efficient, translatable or representative. A few important factors to strive for in a good model would be high permissiveness to infection, human tissues to reflect human intracellular dynamics and representation of all the cells found in normal human lung tissue. Here, we investigated the possibility to use human immortalized cell lines and optimized the permissiveness to infection by transducing the cell lines with SARS-CoV-2 entry factors Ace2 and TMPRSS2.

4.1.1 Vero E6 cells as a positive control to monitor SARS-CoV-2 infection

The green monkey kidney cell line Vero E6 is well described and commonly used as an in vitro model for SARS-COV-2 infection due to its permissiveness to infection and virus replication^{83,53}. Therefore, Vero E6 cells were used to set up infection assays and test the readout techniques. SARS-CoV-2 infection in Vero E6 cells was observed using confocal imaging and flow cytometry. To ensure the structural integrity of the cells was not interrupted and to define individual cells, the cells were stained with a nucleus marker (DAPI), and a marker for actin (Phalloidin). An anti-spike antibody with secondary PE-conjugated antibody was added to indicate infection. Analysis of the infected Vero E6 cells by confocal microscopy revealed infection with both the NL2020 as well as the Patient1 strain, as was demonstrated by clear spike staining in all conditions aside from the mock-treated condition (figure 8). The absence of a spike signal in mock-treated condition showed that the readout technique was specific enough to detect infection. Additionally, the MOI used was sufficient to cause a high infection rate. Together, these results indicate that the infection protocol and readout assays are adequate to distinguish SARS-CoV-2 infection.

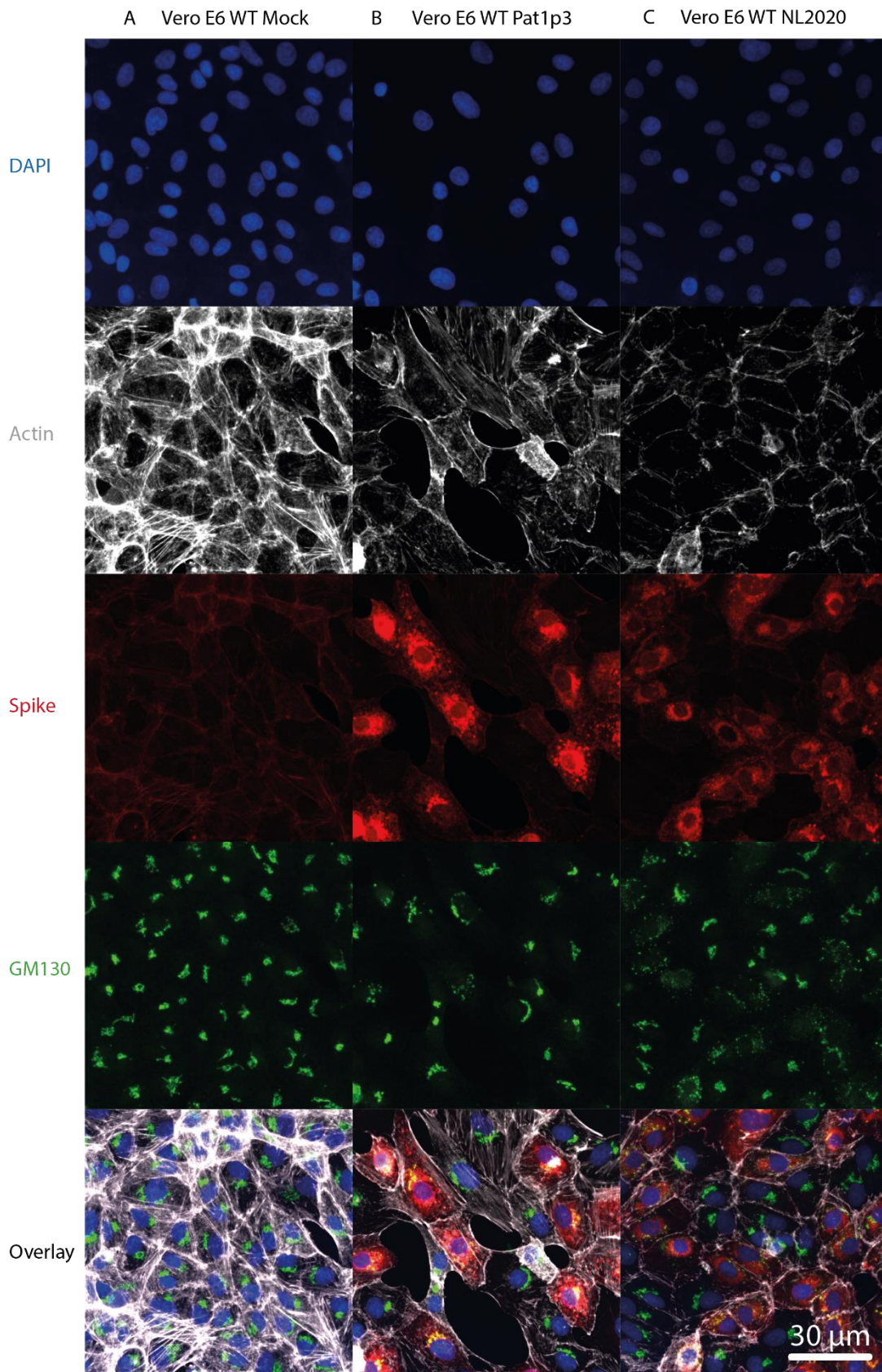


Figure 8: SARS-CoV-2 strains NL2020 and P1P3 efficiently infect Vero E6 cells. Immunofluorescent imaging of indicated markers in Vero E6 cells seeded on an 18 mm coverslip and infected with two strains of SARS-COV-2: Patient1p3 (B) and NL2020 (C), MOI 0.1. Cell morphology was visualized with nucleus marker DAPI (blue), Actin marker (grey) and Cis-Golgi marker GM130 (green). SARS-CoV-2 infection was detected using anti-spike staining (red). The scale bar is 30 μ m. Panels were made with a Zeiss LSM880 Fast Airyscan Microscope. Cells were fixed at 2 dpi.

Next, infection with the NL2020 and GFP strain was confirmed in Vero E6 cells by detecting Spike protein on the cell surface of infected cells, compared to uninfected cells, using flow cytometry (figure 9). As a control to exclude aspecific binding of the secondary antibody, the secondary antibody was added without the primary antibody (figure 9, orange peak). Two days post-infection (DPI), 91% of the cells displayed increased cell surface spike levels in comparison to uninfected cells, confirming that a high percentage of cells were infected (figure S1). Interestingly, two peaks could be observed, discriminating between cells expressing high levels of spike and cells expressing low levels of spike (figure 9). This might reflect the point of the infectious cycle that the cells are in. The time of harvest greatly impacted the amount of detectable spike-positive cells, as demonstrated by the difference in spike expression between one DPI, with almost undetectable amounts of spike-positive cells, and two DPI, with a high proportion of spike-positive cells in the cell population (figure 9). For this reason, an incubation time of two DPI was implemented for future experiments.

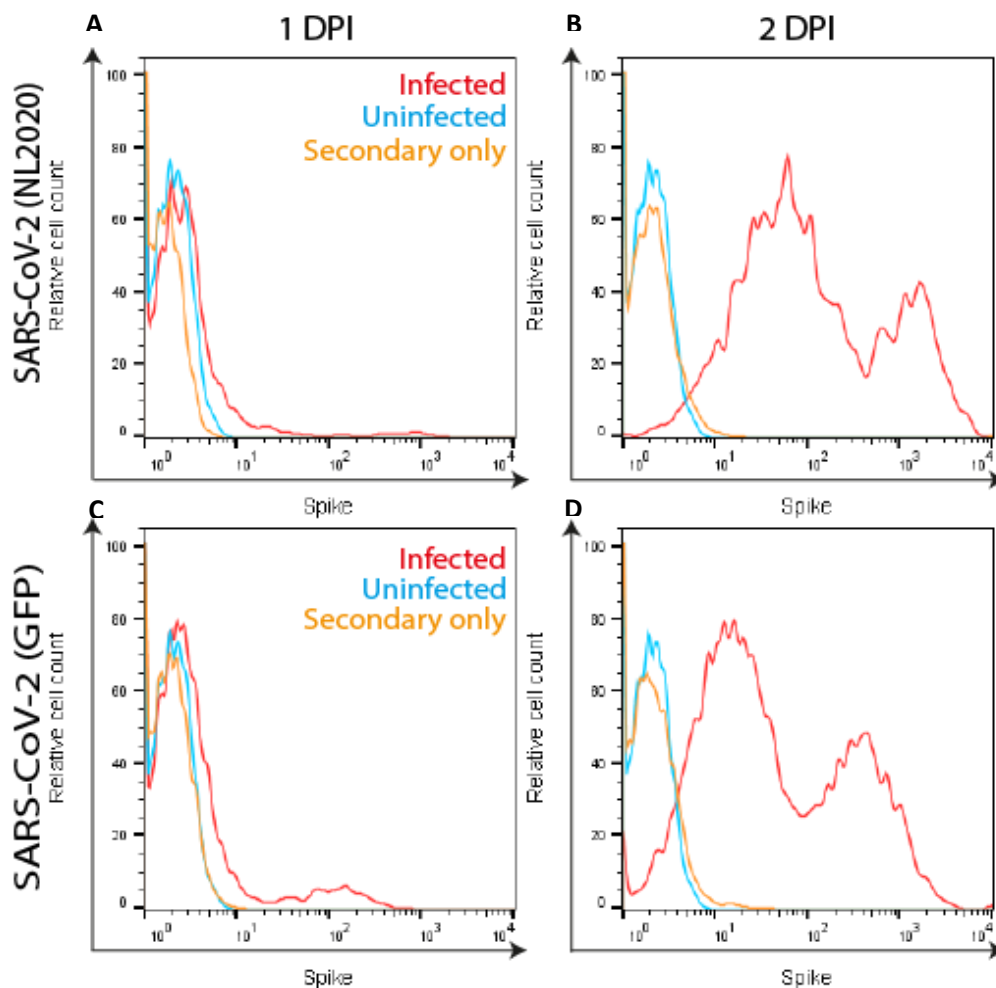


Figure 9: High expression levels of Spike on the cell surface indicate high infection rates in Vero E6 cells at 2 dpi. Flow cytometric analysis of cell surface Spike expression in Vero E6 cells. Cells were infected with two SARS-CoV-2 strains: NL2020 (A, B) and GFP (C, D) (MOI 0.05). The cells were harvested at different time points post-infection: 1 (A, C) and 2 dpi (B, D), and stained with a spike-specific antibody and secondary PE-conjugated antibody. Infection rates were measured by assessing the difference between spike-expression on the cell surface (X-axis) in the infected condition (red) and uninfected/secondary only condition (blue/orange).

These results indicate that Vero E6 cells can be used as a positive control for infection experiments with other cell lines. In addition, because of the high virus production from Vero E6 cells, they are often used to multiply the virus for academic research purposes.

4.1.2 Infection with SARS-COV-2 in Vero E6 cells results in Golgi-dispersion

In the past, different viruses including Influenza A, Polio and HSV-1 have been described to disrupt and disperse the Golgi compartments of infected cells^{84,85,86}. To detect a possible influence of SARS-COV-2 infection on Golgi structure, Vero E6 cells were infected. As stated previously, Vero E6 cells originate from monkey kidneys and might therefore not optimally reflect the human intracellular environment, however at the timing of this experiment, there were no better highly infectable alternatives available. The cells were stained with anti-spike and anti-GM130 (Cis-Golgi marker), and analyzed using confocal microscopy (figure 10). As expected, a high percentage of infected cells was observed, demonstrated by the visible spike staining. Interestingly, in virus-infected cells, the Golgi was more dispersed as compared to uninfected cells. Additionally, virus-infected cells were stretched out. This difference in morphology appeared after infection with both the NL2020 strain and the GFP strain, whereas the

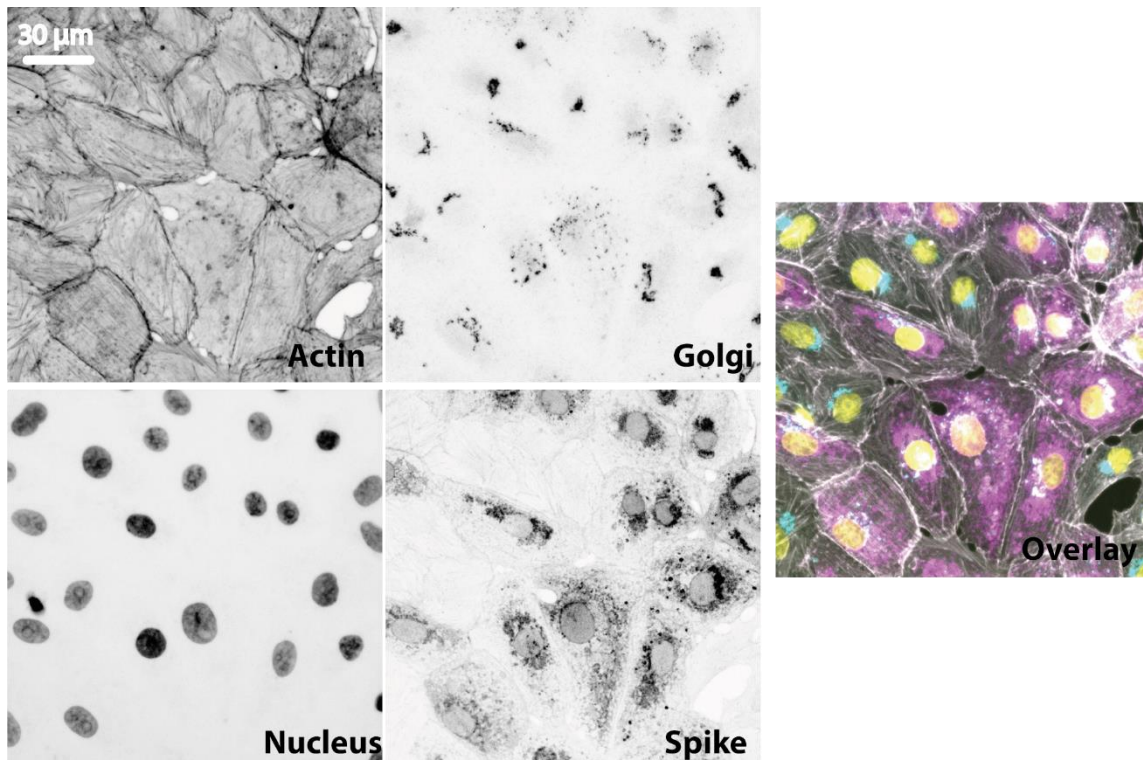


Figure 10: Infection with SARS-COV-2 (Pat1P3) results in Golgi dispersion and a stretched out cell-morphology. Immunofluorescent imaging of Golgi marker GM130 (blue) shows Golgi dispersion in infected cells, visualized by anti-spike staining (purple). Cells become bigger and stretched out, this morphology is visualized with nucleus marker DAPI (yellow), and Actin marker (grey). Scale bar is 30 µm. Panels were made with a Zeiss LSM880 Fast Airyscan Microscope. Cells were fixed at 2 dpi.

Golgi and cells had a normal morphology in the uninfected condition (figure 8). To find out more about the SARS-CoV-2 interaction with the Golgi, other Golgi and ERGIC markers were used to visualize the process. Unfortunately, the background staining from these markers was too high to make clear conclusions from the confocal images. Nevertheless, the differences in cell morphology and GM130

distribution suggest that the principle of Golgi manipulation observed with other viruses also applies to SARS-CoV-2.

4.1.3 Human immortalized cell lines present low SARS-CoV-2 infection rate

SARS-CoV-2 research was not exclusively performed on Vero E6 cells, there are human cell lines that have been used to study SARS-CoV-2 infection or replication^{87,88}. Hence, three frequently described cell lines were tested for their permissiveness to SARS-CoV-2 infection; Huh7 (human liver cells), Caco-2 (human colon cells) (figure 11) and Calu-3 (human lung adenocarcinoma)(data not shown). Additionally, A549 (figure 11), MelJuSo (figure S3) and HEK293T (figure S3) cell lines were tested, because they were available in the lab and easy to transduce. To find out if these cell lines are sufficiently permissive to SARS-CoV-2 infection to efficiently use in a screening platform or a mechanistical assay, they were seeded and infected with SARS-CoV-2. Subsequently, the cells were stained with primary anti-spike and secondary PE-conjugated antibodies, and spike surface expression was tested with flow cytometry. A common factor impeding a clear read-out from the flow cytometer was that the Huh7, Calu-3 and Caco-2 cells clumped together when detached and fixed. As a result, the majority of Huh7 cells were lost in the staining process. The Calu-3 cell clumps became too big to analyze without

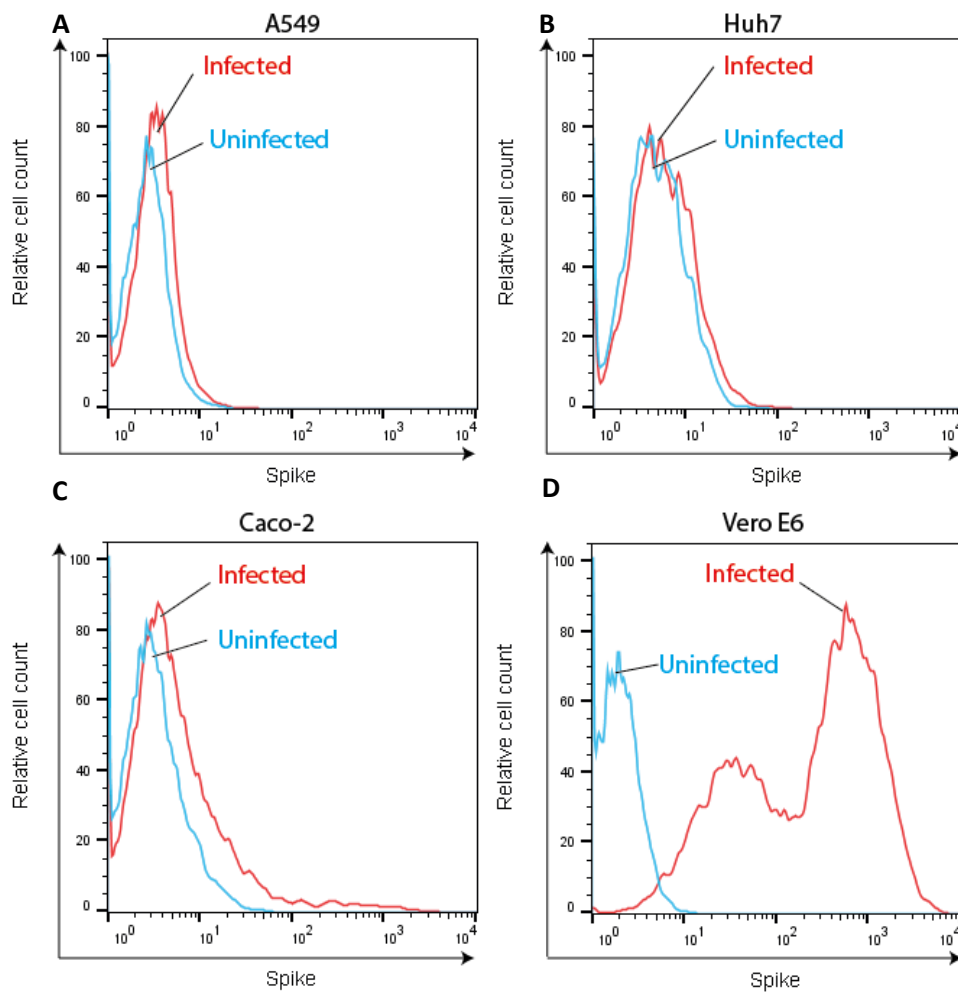


Figure 11: SARS-CoV-2 (NL2020) ineffectively infects human-derived cell lines. Flow cytometric analysis of cell-surface spike-expression in A549 (A), Huh7 (B), Caco2 (C) and Vero E6 (D) cell lines infected with the SARS-CoV-2 NL2020 strain (MOI 0.05). The cells were harvested and analyzed at 2 dpi. Spike-expression on the cell surface was detected by primary anti-spike and secondary PE-conjugated antibodies. One representative experiment of N=2 is shown.

clogging the flow cytometer. Analysis of the remainder of the Huh7 cells and A549 cells showed that a majority of the cells was not infected based on a spike-specific cell surface staining. The Caco-2 cells showed a slight upward shift in spike expression, suggesting that only a small percentage of the cells were infected at MOI 0.05 (figure 11). Contrarily, Vero E6 cells demonstrated a high spike expression, despite being infected with the same MOI, indicating that there was indeed sufficient virus in this setup to cause infection. Thus, these cell lines are not directly useful for infection experiments with this setup.

4.1.4 Improving expression of SARS-CoV-2 receptors Ace2 and TMPRSS2 using lentiviral transduction.

Genetic analysis of the SARS and SARS-CoV-2 spike proteins by Hofmann and colleagues showed that residues described as being important for Ace2-binding were highly conserved in SARS-CoV-2 Spike protein. Additionally, TMPRSS2 inhibitor treatment and transient expression of Ace2 revealed that ACE2 and TMRPSS2 expression are essential for SARS-CoV-2 infection⁵³. Low expression of ACE2 & TMPRSS2 in the tested cell lines could be the reason for their non-permissiveness for infection. To test this hypothesis, TMPRSS2 protein expression on the cell surface was measured using flow cytometry (figure 13). To detect TMPRSS2 cell surface expression, primary anti-TMPRSS2 and secondary PE-conjugated antibodies were added. To exclude aspecific binding of the secondary antibody, only the

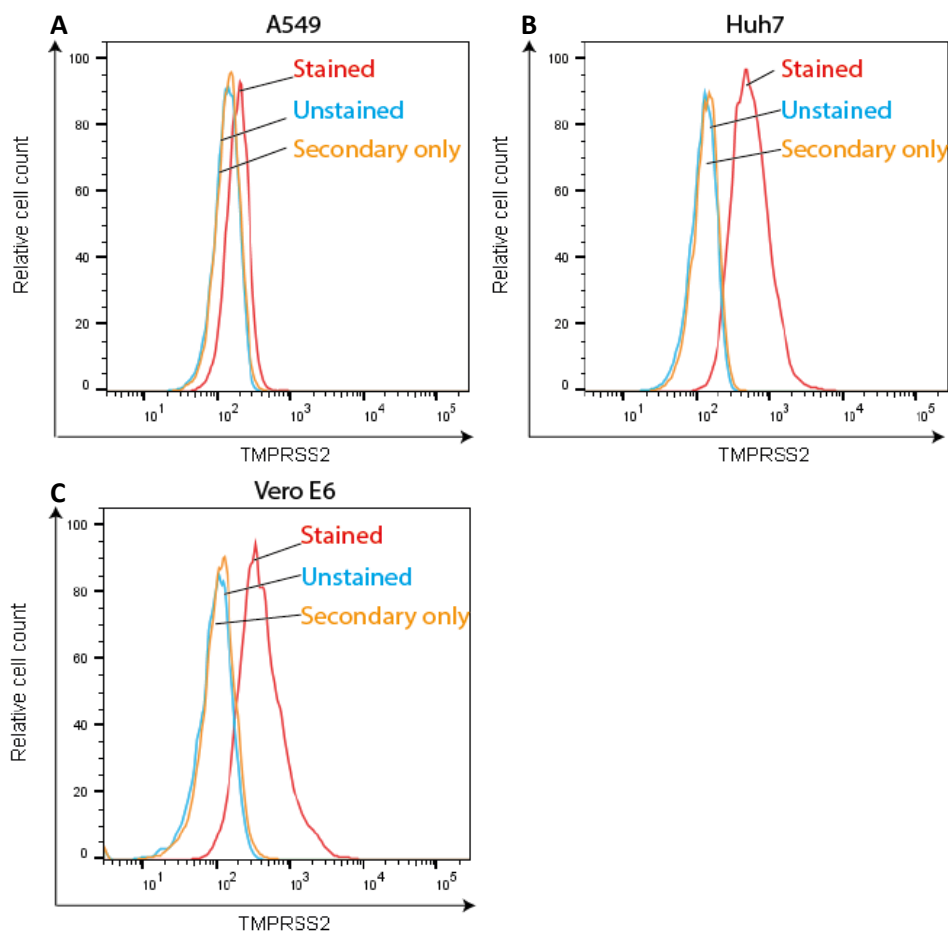


Figure 13: Flow cytometric analysis reveals high TMPRSS2 protein levels on the cell surface of SARS-CoV-2 permissive cell lines. Flow cytometric analysis of PE signal created by primary anti-TMRPSS2 and secondary PE-conjugated antibodies. TMPRSS2 cell surface expression of wildtype A549 (A), Huh7 (B) and Vero E6 (C) cells are measured.

secondary antibody was added in one condition (figure 13, orange peak). As expected, the Vero E6 cells, permissive to SARS-CoV-2 infection, showed higher TMPRSS2 cell surface expression (figure 13). Moreover, Huh7 cells had a very high TMPRSS2 expression profile, whereas other cell lines showed lower TMPRSS2 expression levels on their cell surface.

The total Ace2 protein expression in the wildtype cell lines was examined by Western blot (figure 14). Actin served as a technical control to verify if an equal amount of cell sample of each cell line was loaded onto the gel. Specific bands of a molecular weight of 100 kDa were detected, giving an indication for the Ace2 expression in the different cell lines (figure 14, lanes 3,5,6,7). The Western blot revealed that all tested cell lines contain endogenous Ace2, however there was a difference in expression. The Caco-2 and A549 expressed a higher Ace2 concentration (figure 14, lanes 5,7), whereas Huh7 contained a slightly lower Ace2 concentration (figure 14, lane 3). This result is consistent with the hypothesis, where the non-permissiveness to infection by A549 cells would be caused by a lack of TMPRSS2 expression. Along the same line, Huh7 cells have sufficient TMPRSS2, however non-permissiveness in this cell line could be caused by a low Ace2 concentration. A note of caution should be added when interpreting these results, as the flow cytometry analysis only shows TMPRSS2 cell surface expression, whereas the western blot includes intracellular Ace2. Therefore, Ace2 expression on western blot does not directly prove cell surface expression. Surprisingly, the cell line most permissive to SARS-CoV-2 infection, Vero E6, contained very little endogenous Ace2. However, it has to be taken into account that the antibody used to visualize Ace2 in the western blot is specific for Human Ace2, and may have a decreased affinity for the monkey Ace2 equivalent. Additionally, the Vero E6 cell line has been described to have a high Ace2 expression^{89,90}. Hence, the results from the Vero E6 cell line should be interpreted with caution. The results suggest that the reason for the low infection rates in all tested cell lines, excluding Vero E6, was an inadequate concentration of either Ace2, TMPRSS or both.

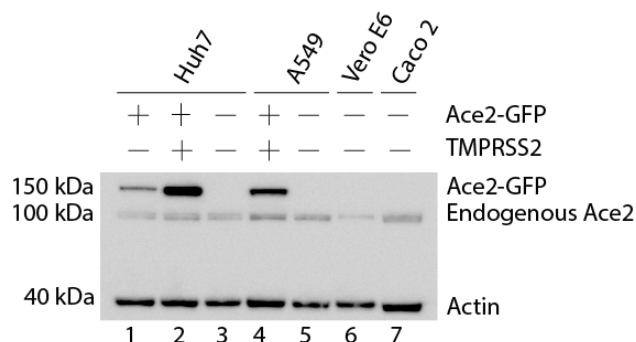


Figure 14: Confirmation of the Ace2-transduction phenotype and endogenous Ace2 expression in wildtype cells. Western blot of endogenous Ace2 (100 kDa) and transduced Ace2-GFP (150 kDa) expression in Huh7 (lane 1-3), A549 (lane 4,5), Vero E6 (lane 6) and Caco2 (lane 7) cell lines. Cell lines were transduced with lentivirus containing vectors for Ace2-GFP (lane 1,2, 4) and TMPRSS2 (not stained, lane 2,4).

High infection rates are fundamental for reliable infection experiments. For this reason, we transduced Huh7, HEK, A549 and Meljuso cell lines with Ace2 and TMPRSS2, consecutively. The described cell lines Calu-3 and Caco-2 were not transduced because they were complicated to culture and seed, which would not serve the purpose of a cell line that can be tested on a large scale. Transduction was first performed with a lentiviral plasmid encoding Ace2 fused to green fluorescent protein (Ace2-GFP). In addition, the lentiviral plasmid encoded a blasticidin resistance gene, which was used to select for transduced cells during 10 days. Then, the cells were transduced with a lentiviral plasmid containing TMPRSS2, provided by Anouk Evers. All transduced cell lines are polyclonal. When looking at GFP-expression, representing the ACE2 construct, all cell lines were between 40 and 60% transduced (Table S1).

To confirm Ace2-GFP protein expression, a Western blot was performed. In the Western blot, Ace2-GFP protein expression would be represented by an additional band of a higher molecular weight (150 kDa), due to the conjugated GFP. Indeed, ACE2-GFP transduced A549 and Huh7 cells contain this additional band when compared to the wildtype A549 and Huh7 cells (figure 14, lanes 1,2,4), indicating that the construct is stably expressed and results in high protein levels of Ace2-GFP. Interestingly, a thicker band in lane 2 and 4 shows that cell lines transduced with both the Ace2-GFP and TMPRSS2 construct contain more Ace2-GFP. Actin served as an internal control, where equal amounts of Actin in all samples indicate equal amounts of input sample. We attempted to perform the same western blot for TMRPSS2 expression, however Western blot anti-TMPRSS2 antibodies did not give specific bands. Unfortunately, there was not enough time to assess TMPRSS2 expression in the transduced cell lines with flow cytometry. Therefore, even though Ace2-GFP transduction was confirmed in the Western blot and TMPRSS2 transduction was performed in the same manner, the effectiveness of the TMPRSS2 transduction cannot be determined with certainty.

4.1.5 Ace2 and TMPRSS2 transduction can effectively increase SARS-COV-2 infection rates in A549 and Huh7 cells

To investigate if the transduced cell lines could reach higher infection levels than the wildtype cells, both wildtype and transduced cells were seeded and infected with SARS-COV-2 (NL2020 and GFP strain). After harvesting and fixation, the cells were stained with anti-spike and secondary PE-conjugated antibodies and analyzed using flow cytometry. The gates indicating spike positive and spike negative cells were determined using uninfected and secondary antibody only controls. Both the A549 and Huh7 cell lines showed an increase in infection after transduction (figure 15). Transduction with both Ace2-GFP and TMRPSS2 improved infection rates from 1% infection to 42,8% in A549 cells (figure 15, A). Interestingly, Ace2-GFP transduction was sufficient for Huh7 cells to become more permissive to SARS-CoV-2 infection, affirming the hypothesis that the previously observed high endogenous TMPRSS2 expression alone is not sufficient for infection permissiveness, but Ace2 addition can improve infection. Despite high expression of the Ace2-GFP construct in the Meljuso and HEK293T cell lines, reflected by a high GFP signal (Table S1), the effect on SARS-CoV-2 permissiveness was limited in these cell lines (figure S4). The fact that Ace2 and TMPRSS2 transduction could only make certain cell lines permissive to infection, hints towards other cell-specific (possibly intracellular) factors influencing SARS-CoV-2 entry, genome translation or replication.

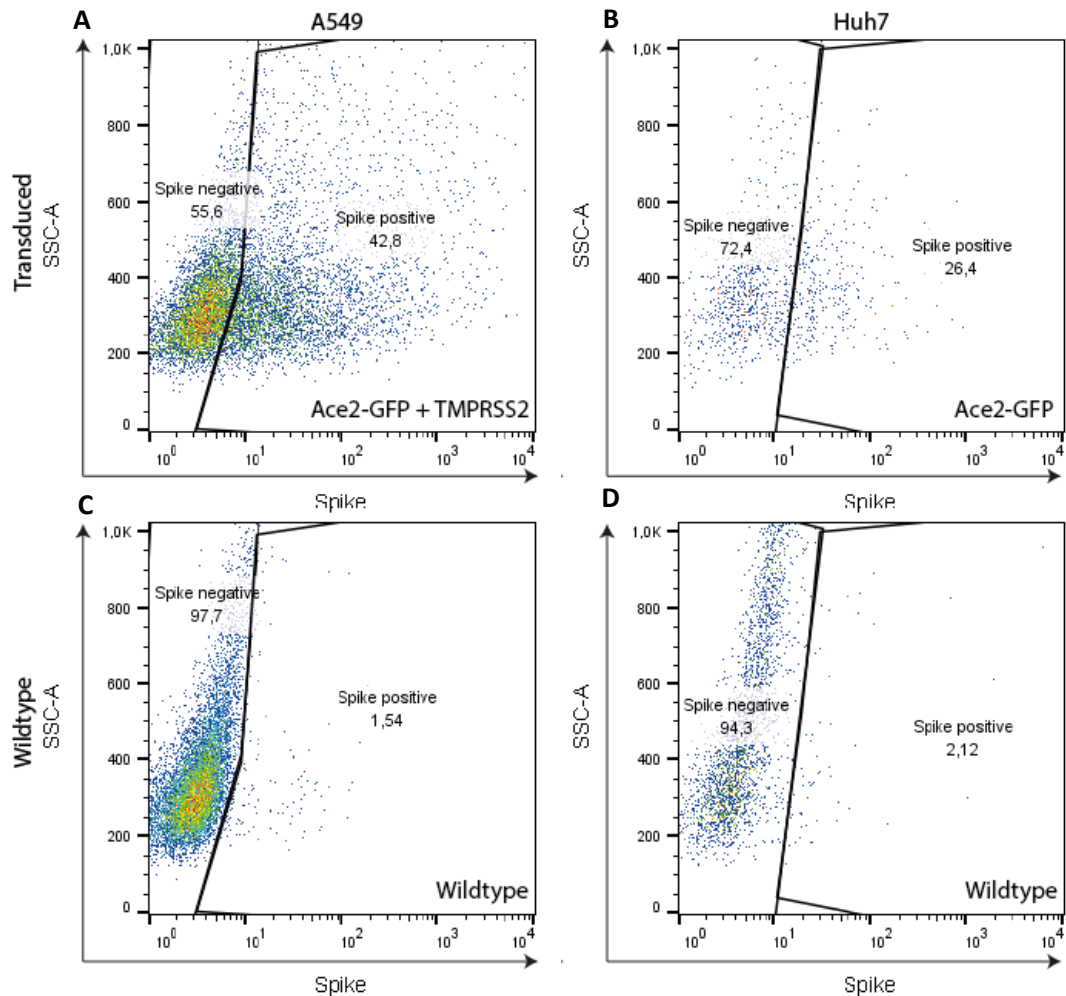


Figure 15: Transduction with SARS-CoV-2 entry factors Ace2 and TMPRSS2 increases permissiveness to SARS-CoV-2 infection in A549 and Huh7 cell lines. Flow cytometric analysis of cell-surface spike expression (X-axis) in transduced (A, B) and wildtype (C, D) cell lines infected with SARS-CoV-2 (NL2020, MOI 0.05). A549 (A, C) and Huh7 (B, D) cell lines were transduced with lentiviral vectors containing Ace2-GFP (A, B) and TMPRSS2 (A). Huh7 cells were only transduced with Ace2-GFP (B). Gates indicating Spike negative and Spike positive cells were set per cell line and the background PE signal was determined using the uninfected and secondary antibody only controls. The numbers within each gate represent the percentage of the total cell population present in the gate.

Permissiveness to SARS-CoV-2 infection is important when cell lines are used as a model. Virus replication is another aspect to study, not only to find out if the viral life cycle is completed, but also to be able to use the cell lines to replicate the virus used for academic research. Currently, Vero E6 cells are used for this purpose, however this method can lead to divergent evolution. The ability of the newly generated cell lines to produce new viral particles determines if the Vero E6 cell lines can be interchanged with transduced human cells in this context. The number of viral particles in the supernatant of transduced and wildtype cell lines was quantified using RT-qPCR (figure 16). The input (grey) was compared to the supernatant of cell lines after 48 hours. The CT-value represents the number of replication cycles necessary to exceed the background threshold, where every replication cycle doubles the number of viral particles. Therefore, a low CT-value represents a high concentration of viral RNA in the analyzed sample. As expected, the golden standard of virus production Vero E6 shows a low CT value compared to the input sample, indicating that the sample contained a high concentration of viral RNA (red). However, the supernatant from the transduced A549 (Ace2-GFP+TMPRSS2) cell line contained an even higher concentration of viral RNA, indicating that this cell line produces large amounts of new viral particles. Additionally, in literature frequently described cell

line Calu-3 showed lower CT-values than Vero E6 without transduction, however this result was less consistent in between both virus strains (figure 16, SARS-CoV-2 GFP). The Huh7 cell line performed very differently with the two virus strains, and it is striking that TMRPSS2 transduction of the Huh7 cell line does not cause it to produce higher virus titers. In conclusion, these experiments indicate that the Ace2-GFP and TMRPSS2 transduced A549 and Huh7 cell lines might represent suitable cell culture models to screen compounds or do mechanistic assays. In addition, Ace2-GFP and TMRPSS2 transduced A549 might provide a better alternative to Vero E6 cells, to replicate SARS-CoV-2 for academic research.

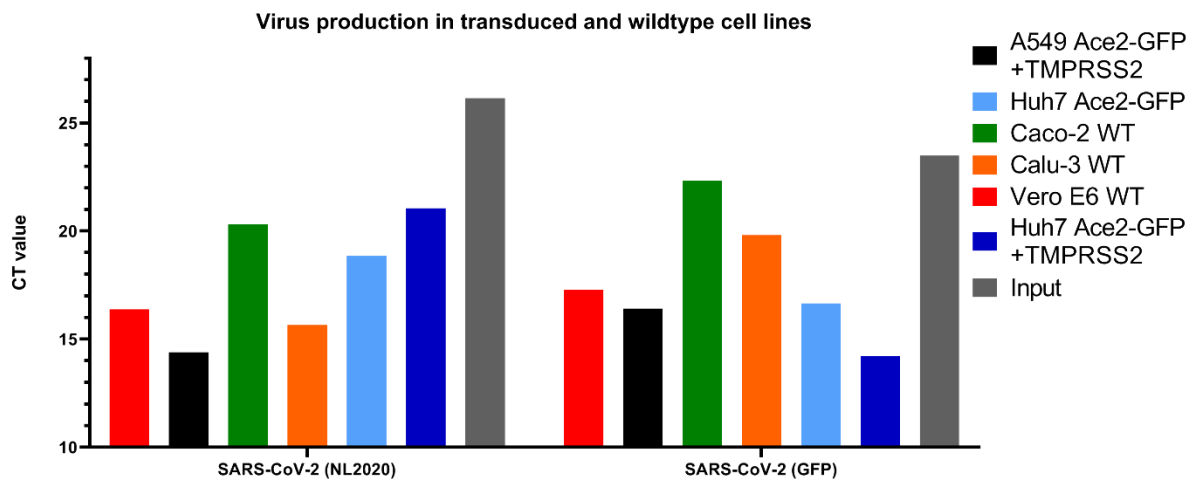


Figure 16: Virus production by wildtype and transduced cell lines. RT-qPCR measurement of supernatant 48 hours post infection, MOI 0.01. Cell lines were infected with SARS-CoV-2 NL2020 (left) and SARS-CoV-2 GFP (right). Input sample (grey) is compared to A549 Ace2-GFP + TMRPSS2 (black), Huh7 Ace2-GFP (light blue), Caco-2 WT (green), Calu-3 WT (orange), Vero E6 WT (red) and Huh7 Ace2-GFP + TMRPSS2 (dark blue). A lower CT-value represents a higher amount of virus recovered from the supernatant.

4.2 Primary cell cultures

Finding appropriate in vitro model systems can require three factors; high permissiveness to infection, human tissues to reflect human intracellular dynamics and representation of all the cells found in normal human lung tissue. The previous results showed that immortalized human cell lines can meet the two first criteria, they will however not comply with the representation of the different cell types found in human lung tissue. Here, we investigate other culture systems that consist of growing and differentiating primary human airway basal cells on ALI filters and developing organoids from them.

4.2.1 Cell types in ALI cultures can be distinguished using flow cytometry

One of the properties that make the Air liquid Interface cell culture system unique is the differentiation of the human primary basal cells to all kinds of different tissue-resident lung cells. Generally, to characterize these different cell types, antibodies against cell-type specific markers are used. However, staining with these antibodies in every experiment would limit the range of combinations of other cell surface markers that can be tested in the same experiment because of a limited amount of isotype combinations. In addition, the differentiation process has a duration of approximately three weeks, which hinders high-throughput screening on these cell cultures. It was previously reported by Dr. Bonser and colleagues, that primary cell cultures can be characterized using flow cytometry⁹¹. If the cell type could be determined by the population shown in the forward/sideward scatter from the flow cytometer, these experiments could provide more information per experiment. To this end, we

harvested the cells from the ALI filters and stained them with antibodies against nerve growth factor receptor (NGFR) and Ezrin. NGFR is a marker for lung progenitor cells, indicating basal cells⁹². Ezrin is a scaffold protein that is involved with microvillus assembly, thereby being mostly present in cells containing microvilli⁹³. Based on the size and granularity of the cells, three clear populations could be distinguished (figure 17, A). The expression level of NGFR and Ezrin was assessed. Population 2 had a lower expression of NGFR than the other two cell lines, whereas the Ezrin expression was very high. The low NGFR level could indicate that this cell population is differentiated, and contains microvilli, which would point towards ciliated cells. Interestingly, populations 1 and 3 both contain high levels of NGFR and low levels of Ezrin, indicating that these populations are both composed of basal cells. However, these populations differ very clearly in size and granularity, indicating that they are two different cell types, nonetheless, these cell markers cannot distinguish between the two. Overall, these results show that growing basal primary cells on Air Liquid Interface filters with specific growth factors can trigger differentiation of the basal cells. In addition, different cell populations can be identified by assessing only the forward and sideward scatter data on the flow cytometer.

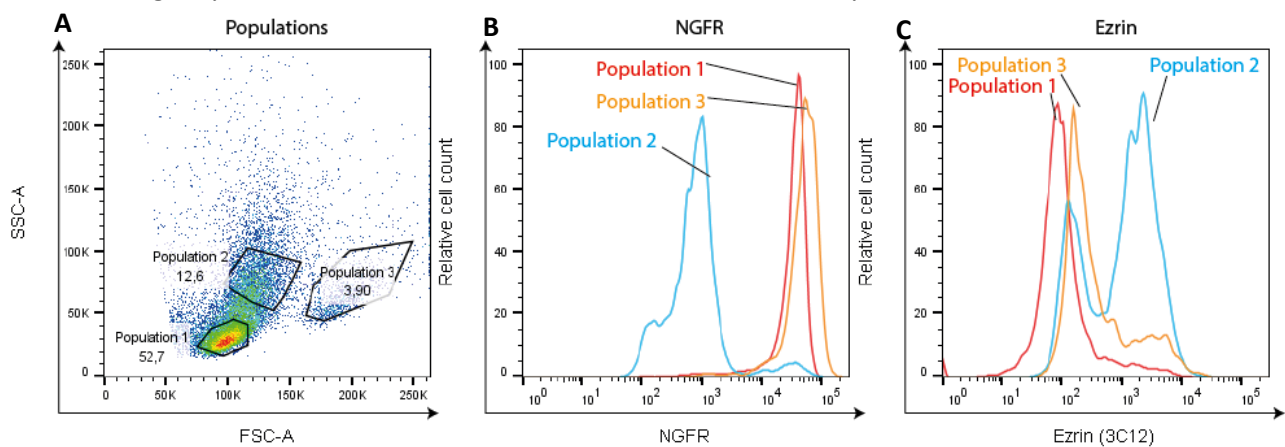


Figure 17: Flow cytometric analysis of ALI cultures shows different cell populations that represent the different cell types of air liquid interface cell cultures. Different populations can be observed when looking at the forward (size) and sideward (granularity) scatter (A). Expression of lung progenitor cell marker NGFR (B). Expression of microvillus marker Ezrin (C).

4.2.2 SARS-CoV-2 can infect Air liquid interface (ALI) cell culture

The ALI culture model system meets two of the previously set criteria for a SARS-CoV-2 model system; it is a primary human cell line, and contains the three most important cell types found in the human airway, as was demonstrated by the characterization of the populations found in the flow cytometer and further explored in other research⁹⁴. To assess the last criterium; permissiveness of the ALI cell culture model to infection, Human Nasal Epithelial (HNEC) cells from two donors were grown on ALI filters, and infected with SARS-CoV-2. After 1,4 and 7 days, supernatant from the apical side of the filter was harvested and qRT-PCR was performed to determine the amount of viral RNA produced by the ALI cells over time (figure 18, A). The qRT-PCR showed a higher CT-value compared to the input sample in all time points, indicating a lower amount of viral RNA present in the sample. This suggested that the sampling method or the time point were not adequate to detect SARS-CoV-2 infection. The experiment was repeated to optimize the virus detection in ALI-grown cultures. In this repeat, the RNA was isolated from the cells rather than collected from the supernatant and samples were taken at earlier time points (figure 18, B). Additionally, a condition was added to test the antiviral activity of adenosine nucleotide analog pro-drug Remdesivir on SARS-CoV-2 infected ALI primary human cell cultures. This new setup resulted in a lower CT value in the hours directly after infection. In line with the previous results, the CT-value increased to approximately input level after 1 dpi. Conditions treated

with Remdesivir showed a consistently higher CT-value than untreated conditions, confirming the reports of Remdesivir inhibiting SARS-CoV-2 replication. Notably, the samples taken at 2 hours post-infection are considered input samples, however they differ in CT-value, possibly indicating a difference in the amount of infectious virus added to infect the cells. Additionally, the ALI cell culture infection rates were variable in other experiments, demonstrating a need to interpret these results with caution. Nonetheless, these results provide a promising start of the usage of ALI-cultured primary airway cells in SARS-CoV-2 research.

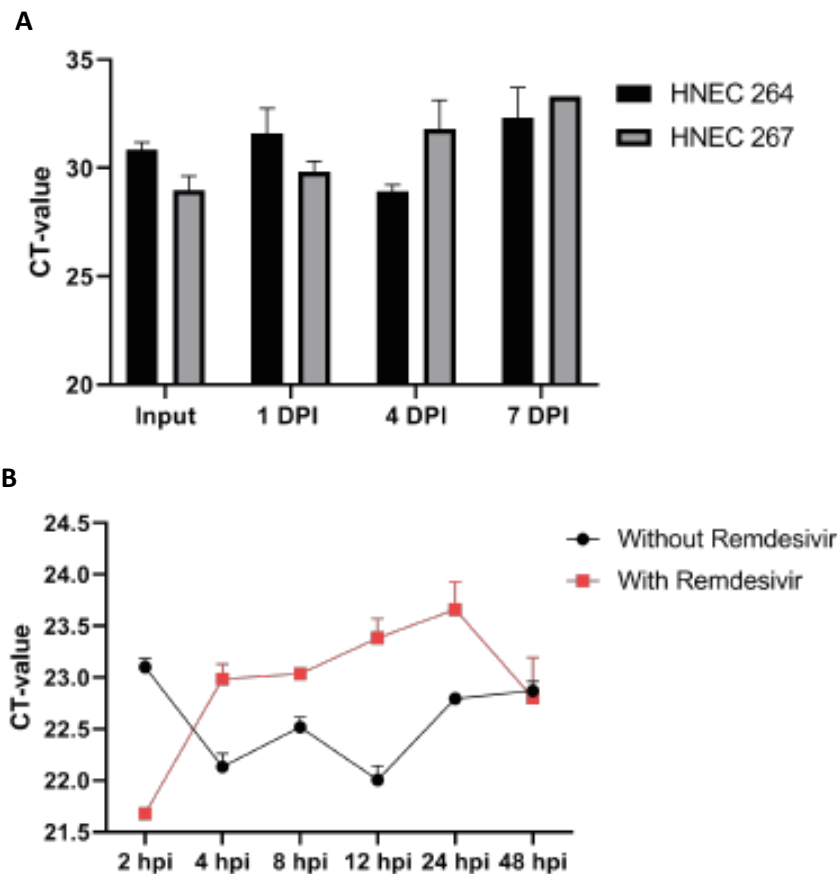


Figure 18: Production of viral RNA by Human Nasal Epithelial Cells (HNEC) can be optimally detected hours after infection and by performing RNA isolation. (A) RT-qPCR of supernatant taken from the apical side of a Human Nasal Epithelial Cell (HNEC) cultures grown on Air Liquid Interface (ALI) filters. HNEC from two different donors (264 and 267) were infected with SARS-CoV-2 (NL2020), MOI 0.01. Sample was taken from the Input and 1,4,7 days post-infection (DPI). Error bars represent technical triplicates. (B) Time-course measurements of viral RNA after RNA isolation from samples at 2 hours post-infection (input) and 4,8,12,24,48 hours post-infection. Samples were infected with SARS-COV-2 (NL2020, MOI 0.01) and treated with (red) or without (black) Remdesivir. Error bars represent technical triplicates.

4.2.3 Using organoids for high-throughput compound screens

As previous experiments show, ALI cell culture models are a promising candidate for new SARS-CoV-2 infection experiments, however they provide a technical draw-back; to develop one filter of differentiated ALI primary cell cultures, at least 3 weeks of differentiation with different media and growing conditions are required. This drastically impacts the speed at which compounds can be tested, and is therefore not directly useful as a screening platform. However, these ALI cell cultures can also be used to develop airway organoids. With this technique, many organoids can result from one filter, with as a result the option to test many conditions instead of one condition per filter. The higher

amount of organoids allows researchers to test more antiviral compounds within the same experiment, which makes the organoid model more suitable for high-throughput experiments.

To assess if the HNEC cells can still be infected and virus can be detected when organoids are formed, organoids were formed in matrix gel on 96-well plates. Subsequently, medium containing SARS-CoV-2 was added to the organoids. After 2 hours, a sample was taken from the matrix that organoids were embedded in, and the medium was replaced. This sample is considered the input, baseline sample. Other samples were taken at different time points (1,2 and 3 DPI). A qRT-PCR was performed to determine the amount of viral RNA present at different time points. Results show a low CT-value, and therefore a high concentration of viral RNA in all time points (figure 19). However, there is no clear and donor-consistent decrease in CT-value between the input sample and the later time points. It could be argued that the virus has been washed away and therefore the low CT-value is due to viral production by the organoids. However, the lack of decrease in CT-value between the input sample (2hpi) and the other time points is consistent between donors and virus strains. Therefore, it suggests that the matrix is able to absorb and contain the virus even through the washing step. Another observation from the qRT-PCR data is that the overall infection rate with the SARS-CoV-2 NL2020 strain is higher than the Pat1p3 strain, and there is no noticeable difference between conventional and inside-out organoids (figure 19). These results implicate that this method does not accurately reflect infection in organoids, therefore it is essential to optimize this process, for example by measuring earlier time points.

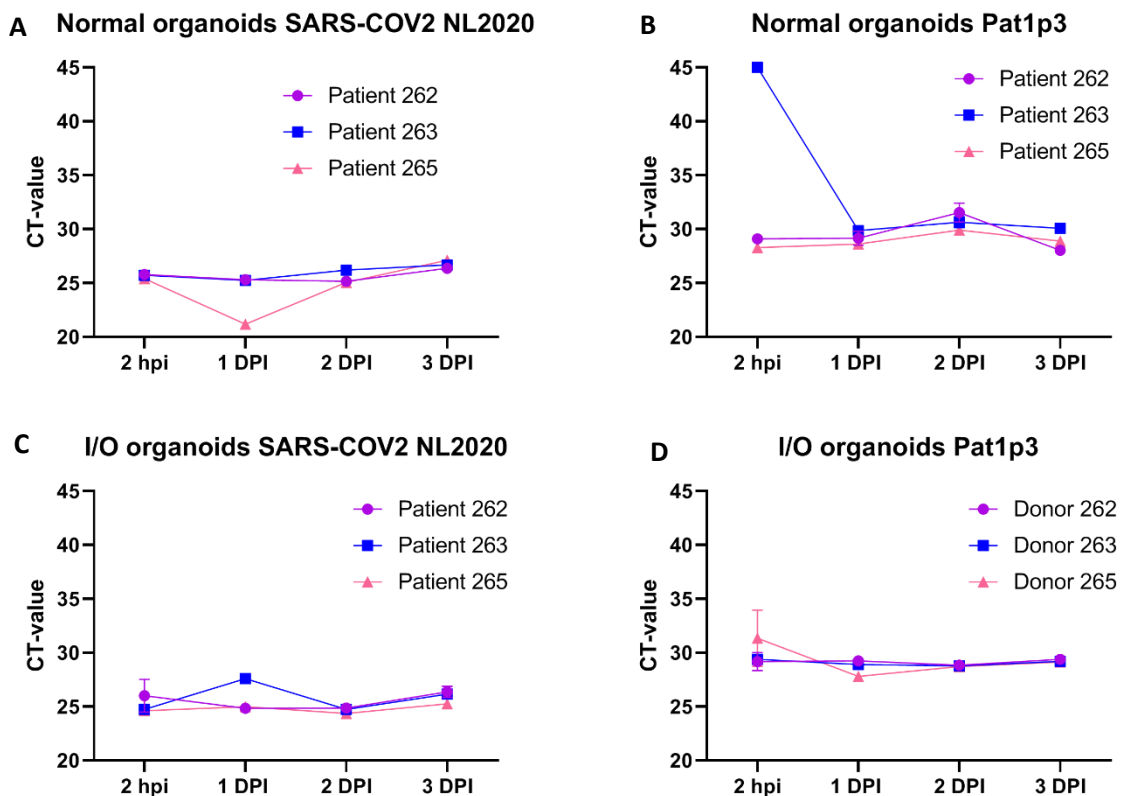


Figure 19: RT-qPCR measurement does not effectively detect SARS-CoV-2 infection in organoids. RT-qPCR measurement after RNA isolation from the matrix that the organoids were embedded in. Organoids were infected with SARS-CoV-2 NL2020, (A,C) and Pat1p3 (B,D) infected organoids 2 hours post-infection (input) and 1,2,3 DPI. Organoids were derived from different donor basal cells, and were divided into conventional organoids (A, B) and Inside out organoids (I/O) (C, D).

4 Discussion

SARS-CoV-2 has had an enormous negative impact on public health, healthcare systems, economy and political stability over the world¹³. Vaccines and therapies are being developed at a fast pace in what seems to be a race against new viral variants appearing. Variants have been reported to have the capacity to bind to human Ace2 receptor at a higher affinity, as well as to be able to partly evade the immunity provided by vaccines and previous infections⁹⁵. This race will continue for the foreseeable future. One of the most important tools to find new therapies or drug targets are in vitro models. In vitro models provide an opportunity for rapid screening of compounds or drug targets, and they have been essential in the development and first stage testing of currently developed therapies⁹⁶. However, the currently used in vitro models can be problematic for a number of reasons. They can differ from the in vivo situation for example in species, permissiveness, or representation of the cells found in normal human lung tissue. As a result, the complexity of a human lung is not represented in the model. This study is aimed to shed light on the advantages and disadvantages of each in vitro model, as well as to optimize the models for SARS-CoV-2 infection.

The currently most frequently used cell culture model for SARS-CoV-2 infection is the Vero E6 cell line. This is a rhesus monkey kidney cell line and contains a different physiology than human cell lines. The Vero E6 cell line is oftentimes used to replicate the SARS-CoV-2 virus in an academic research setting due to its potential to produce high viral titers⁷². We confirmed that Vero E6 cells are indeed highly permissive to infection, even with a low MOI of 0.05. The MOI is a crucial aspect of the permissiveness of cell lines. Although the Vero E6 cell line has been reported to be highly permissive in a range of different MOIs, the permissiveness of other cell lines has been debatable. The MOI used and described in literature can range from a very low MOI (0.001) to a very high MOI (5)^{97, 98}. This is a plausible explanation for our results contradicting the reports about permissiveness of the same cell lines, for example wildtype Calu-3, Huh7 and A549⁹⁹.

There has not been a clear consensus over what MOI would accurately mimic the in vivo situation, and therefore it is difficult to make a recommendation on a general MOI to use for SARS-CoV-2 infection experiments. There are some discussion points to consider. The first consideration is that if a very high MOI is added, chances are that all the cells in a sample will get infected, which would provide a high amount of infected cell sample for analysis. A disadvantage of this approach would be that if all cells are infected at the first addition of the virus, only the first infectious cycle can be studied. Contrarily, if a very low MOI is used, viral production and subsequent viral spread can be studied, on the other hand, it will be more difficult to find significant results with a very low infection rate. Additionally, it is important to consider the interaction between virus particles. It has been reported that the Vesicular Stomatitis Virus (VSV) can form multi-virion infectious units that infect the cell as one unit¹⁰⁰. If SARS-CoV-2 possesses the same properties, this interaction would have a high probability of happening when using a high MOI, thereby producing a non-specific outcome from the conditions tested. On the other hand, if these infectious units are also formed by the SARS-CoV-2 virus, they might represent a biologically relevant mechanism. These factors can have a considerable impact on experimental outcomes and should be weighed in when calculating an MOI during experiment design.

To calculate the MOI, the number of infectious particles is divided by the number of cells in the well. Two frequently used ways to determine and calculate the number of infectious virus particles in a stock are the plaque assay; determining plaque-forming units (PFU) and the Tissue Culture infectious dose; resulting in the concentration at which 50% of the cells show cytopathic effect (TCID50)^{101,102}. The original method for calculating the TCID50 described in the virology guide of the ATCC, was developed by Reed and Muench and is still being used today¹⁰³. From the TCID50, it is

possible to deduce an estimate of the PFU, where the $PFU = 0.7 * TCID50^{104}$. Another method for TCID50 calculation was described by Spearman and Kaerber, resulting in a different PFU/TCID50 ratio of around 0.56¹⁰⁵. This method was reported to more accurately represent the amount of infectious viral particles in a sample¹⁰⁵. Nevertheless, the most accurate finding of the PFU would be a direct experimental measurement from the plaque assay. This was shown in a side-by-side comparison between the two techniques in filoviruses¹⁰⁶. For the purposes of this thesis, the calculation method is less relevant because the comparisons between cell models were made using the same virus stock, however it is the reason why it is difficult to compare the results from different strains e.g. the patient1, GFP and NL2020 strain. Moreover, to ensure consistency in SARS-CoV-2 research, it is important to be mindful of the differences in viral particle calculation.

Another aspect to consider when interpreting the SARS-CoV-2 infection results is what proportion of the detected viral activity is active replication. Importantly, it has been reported that Hepatitis B virus-infected cells produce virions without a viral genome¹⁰⁷. Similarly, defective interfering particles (DIP) are commonly described after passaging Influenza A virus^{108,109}. DIP contain smaller units of the standard Influenza genome and are dependent on co-infection to replicate. In this thesis, the detection of the spike protein on the cell surface is considered a sign of viral infection of the cell. It could be argued that if the virus stock contains virions without a (complete) viral genome, the fusion of the viral envelope with either the cell membrane or the endosomal membrane could still result in spike-expression on the cell surface after endosome recycling. Presumably, this expression would be too low for detection and the proportion of empty virions is the same when the same virus stock is used. That is why this factor is neglected for the purpose of this thesis. Yet, the scenario should especially be considered when comparing experiments from different virus stocks, albeit that this phenomenon has not been described for SARS-CoV-2 thus far.

The infection rate and viral production were also measured with RT-qPCR. This technique detects the viral RNA encoding the Envelope protein, one of the genes that can be translated from subgenomic RNA species¹¹⁰. These RNA species are generated by nested replication of negative sense replication intermediates. Although the detection efficiency of these subgenomic RNAs with RT-qPCR is not exactly described, it has been reported that their detection is not a good indicator for active replication¹¹⁰. The detection with RT-qPCR may depend on the source of the sample taken. In most of the experiments we described, a sample was taken from the supernatant, which should not contain a high amount of intracellular proteins and genetic material except for the excreted virus. An exception would be when cells show high cytopathogenic effects or secrete virions without a viral genome. Therefore, in the case of a sample taken from the supernatant, theoretically only RNA from the viral particles will be present in the sample. When taking a cellular sample and isolating the RNA from this sample, this could contain different RNA intermediates and subgenomic RNAs, which might result in an inaccurate measurement. An additional note regarding the RT-qPCR results is that when comparing the difference between virus strains it has to be taken into account that each strain is derived from a different stock. Although the input is carefully calculated, the margin of error will be higher, because all virus strains will have a different mastermix, this was demonstrated by the difference in CT-value between SARS-CoV-2 input samples in figure 18. Although the calculations and appropriate controls were included to minimize the influence of these factors, they should be considered when drawing conclusions from RT-qPCR results.

Granted that the previously discussed drawbacks are valid in the context of individual experiments, the overall conclusion can be drawn that the methods used for virus infection and detection are robust when combining results from confocal imaging, flow cytometry and RT-qPCR. However, the infectiousness of the SARS-CoV-2 GFP strain could be debated. The presence of spike

protein on the Vero E6 cell surface indicates infection by the GFP strain, yet this result was not confirmed when measuring the eGFP integrated into the genome of the SARS-CoV-2 GFP strain (figure S2). One possible explanation for this discrepancy could be that the GFP fluorophore was weakened by formaldehyde fixation, as was described previously by Stewart et al¹¹¹. This hypothesis is strengthened by the observation of a clear GFP signal when the cells are inspected in the microscope inside the BSL3 lab, whereas this signal could not be observed anymore after the removal from the BSL3 lab and corresponding formaldehyde inactivation of the sample.

Despite the discrepancy in GFP-signal, with the used protocol, confocal imaging and flow cytometric analysis demonstrate high infection rates with all virus strains in Vero E6 cells (figure 8 and 9). The infection experiments with Ace2- and TMPRSS2-transduced cells indicate that introduction of Ace2 and TMPRSS2 can improve SARS-CoV-2 infection efficiency in immortalized cell culture models. Considering that some of the tested cell lines remain uninfected even after the addition of the entry receptor and protease, it is probable that infection depends on more host factors. Several high-throughput CRISPR-knockout screens were recently performed, where potential host factors essential for SARS-CoV-2 infection were found¹¹². For instance, histone modification and chromatin regulation factors, including the SWI/SNF complex, were identified as genes increasing SARS and SARS-CoV-2 infection, suggesting an important role for SARS-CoV-2 proteins in epigenetics⁹⁰. Another wide-scale protein interaction screen implied a role for SARS-CoV-2 protein ORF10 in the ubiquitination pathway⁸³. These factors need to be investigated in further detail to explain the uninfected cell lines and can potentially represent a new Achilles heel of the virus in finding better therapeutic strategies.

Our confocal imaging results showed that SARS-CoV-2 infection can lead to Golgi dispersion. Indeed, a few weeks after we obtained these results, they were confirmed by a study from Dr. Cortese et al, showing that SARS-CoV-2 infection leads to extensive Golgi fragmentation together with cytoskeleton remodeling and the formation of double-membrane vesicles¹¹³. Although this is a more broadly found mechanism in several different viruses, it is an important piece of the puzzle regarding the SARS-CoV-2 viral replication cycle. The fact that this phenomenon was described in several different unrelated viruses, shows that remodeling of cellular structures provides the virus with an evolutionary advantage^{86,84}. This might not be surprising, considering that Golgi morphology has been shown to have a direct influence on important cell processes such as apoptosis, stress responses and cell polarization¹¹⁴. Targeting these cell processes through Golgi-dispersion could provide SARS-CoV-2 an evolutionary advantage. Additionally, Golgi cell membranes have been reported to be part of the replication/transcription complex (RTC), providing protection for the viral RNA during transcription and replication¹¹³. An important side note to provide here is that Golgi-dispersion after viral infection has been reported to be cell-type dependent, as some cell types did not present the same phenotype after HSV-1 infection⁸⁶. To make sure this phenotype is a biological consequence of SARS-CoV-2 and not a Vero E6-specific artifact, we performed the same experiment in human cell lines⁹⁴. The results confirmed that the phenomenon of Golgi-dispersion is universal for the cell lines tested.

The SARS-CoV-2 infection models described in this thesis have been focused on improving the cell culture system that infection takes place in. Another variable in model systems is the virus that is used. Importantly, research on SARS-CoV-2 biology needs to be performed in the BSL3 lab, providing limited time conditions and experimental possibilities. Only a limited amount of groups have access to BSL3 labs. In an attempt to tackle this time-consuming step, Bloom and colleagues described a new option to perform neutralization assays for SARS-CoV-2 under BSL2 conditions, using SARS-CoV-2 spike-Pseudotyped lentivirus⁸². This lentivirus contains SARS-CoV-2 spike protein on the envelope, but does not carry any SARS-CoV-2 RNA or other SARS-CoV-2 proteins, hence the virus is safe to use under BSL2 conditions. Unfortunately, we were unable to achieve infection with the spike-Pseudotyped virus

(data not shown). However with more time, the system shows great potential and can be especially useful in neutralization assays, or testing compounds that have a function in limiting virus entry.

Until recently, the majority of SARS-CoV-2 research was performed either in Vero E6 cells or in human immortalized cell lines using a high MOI¹¹⁵. The need for more translatable in vitro cell models was distinctly demonstrated during the process of chloroquine and hydroxychloroquine repurposing for SARS-CoV-2 treatment. Based on research in Vero E6 cells, chloroquine and hydroxychloroquine were described to be effective inhibitors of SARS-CoV-2 replication¹¹⁶. Conversely, during patient trials, this protective and antiviral effect was not reflected in a decline in severe disease or incidence of death^{117,118}. One of the hypotheses for this inconsistency was that the SARS-CoV-2 Spike protein activation and subsequent membrane fusion was mediated by different proteases in vivo as opposed to in vitro¹¹⁹. Hydroxychloroquine and Chloroquine are reported to work as a lysosomotropic agent, where they elevate the pH in lysosomes and endosomes, thereby abrogating the function of endosomal protease Cathepsin L¹²⁰. To activate membrane fusion and infection, SARS-CoV-2 Spike cleavage needs to occur. In SARS-CoV-2 as well as other coronaviruses, this cleavage can be performed by Cathepsin L, demonstrating the antiviral mechanism of hydroxychloroquine and chloroquine in vitro⁵². As mentioned before, in SARS-CoV-2, Cathepsin L can be redundant when TMPRSS2 is present, strengthening the hypothesis that the efficacy loss of hydroxychloroquine and chloroquine in vivo is caused by SARS-CoV-2 entering independently of Cathepsin L activity^{53,119}. This difference could have been detected earlier if the in vitro models had contained proteins reflecting the in vivo lung cells. Arguably, the immunomodulatory functions of hydroxychloroquine and chloroquine on lymphocytes and macrophages could also impact COVID-19 progression, however any functions working on immunity other than cell-intrinsic immunity would not have been represented in the initial in vitro models, because of the lack of immune cells¹²⁰. These arguments emphasize the need for refined in vitro models, especially with cell types representative of the human lung epithelium, and possibly with components mimicking the immune system.

There have been reports of primary cell cultures and organoids being used in SARS-CoV-2 research¹²¹. This thesis can elucidate the advantages and disadvantages of the use of these models in different experiments and settings. Furthermore, the models described here could be improved upon by including components from the immune system. It has been described previously that SARS-CoV-2 and other pathogenic coronaviruses can evade and manipulate the immune system by interrupting the Interferon response or HLA presentation^{122,123}. In addition, the immune response contributes significantly to SARS-CoV-2 pathology¹²⁴. Immune evasion by SARS-CoV-2 and immune involvement in SARS-CoV-2 pathology indicate that host-pathogen interactions are important potential subjects of future research. By adding immune cells to cell culture models, it might be possible to mimic immune pathology and host defense responses. The co-culturing of immune cells was proven valuable in allergic contact dermatitis research, where heterotypic cell-cell interactions were studied by co-culturing dendritic cells with keratinocytes¹²⁵. Similar approaches have been taken in cancer research, where 3D multicellular tumor spheroids are infiltrated by monocytes to mimic interactions between immune cells and the tumor micro-environment¹²⁶. Further research is necessary to explore which components of the immune system can be introduced in the different in vitro cell systems. In addition, there are other in vitro model systems that can be considered for SARS-CoV-2 infection experiments and immune cell co-culturing, such as the Organ-on-Chip model¹²⁷. Overall, the model systems developed and described will provide a possibility to perform future research with more translatable results, which will contribute to an increased understanding of SARS-CoV-2 biology and may lead to development of compounds active against SARS-CoV-2.

5 Conclusion

In order to find new SARS-CoV-2 therapies, vaccines and knowledge of the viral infection cycle, translatable in vitro cell models are indispensable. The presented results show that there are at least four different in vitro models that can be used in experiments with SARS-CoV-2. Each model has advantages and disadvantages that should be taken into account when an in vitro model is chosen for experiments. The first possibility that was discussed was the Vero E6 cell line, these cells are highly permissive, even at a low MOI. However, they are not of human origin and have been reported to drive divergent evolution^{73,74}. Therefore these cell lines are not optimal for virus production, and an alternative was searched for. The second model that was discussed was the human immortalized cell line. These cell lines improve upon Vero E6 cells because they are of human origin, but they were difficult to infect with SARS-CoV-2. We transduced these cell lines with SARS-CoV-2 entry factors Ace2 and TMPRSS2, which effectively increased the SARS-CoV-2 permissiveness of the cell lines. Transduction of A549 or Huh7 also led to higher virus production, allowing for these cell lines to be used as an alternative to Vero E6 cells in virus production. The immortalized and transduced cell lines are very useful when looking at general cellular functions, however they do not represent all the differentiated cells of the lung epithelium. To study SARS-CoV-2 infection in these cells, primary HNEC cells can be differentiated on an ALI filter. This results in the development of mucin-producing goblet cells, ciliated cells, basal cells and club cells. We showed how the different cell populations can be detected using only the forward and sideward scatter of the flow cytometer and how the HNEC cells can be infected. These ALI cell culture models are very useful for experiments where different cell types are required, however the development of a single ALI filter takes at least three weeks. This is a substantial disadvantage when a high-throughput system is necessary. Therefore, we considered the use of organoids. A considerable advantage these organoids is the high-throughput potential they harbor. Namely, one ALI filter can provide several organoids, thereby making a single condition in these organoids a lot less time-consuming. However, our results showed that it is difficult to detect infection in these organoids and there is a need to optimize this system. Overall, the results show that the choice of model system is an important and often underestimated part of designing experiments. The model system can have an unintended impact on experimental conditions and results.

6 Acknowledgements

During my internship and the writing of this thesis, I received a great amount of support and guidance. Firstly, I would like to express my sincere gratitude to Dr. Patrique Praest for the daily supervision, feedback and enthusiasm. In addition, I would like to thank Dr. Robert Jan Lebbink and Prof. Dr. Emmanuel Wiertz for the opportunity to work in their lab and the interesting discussions and advice during the work meetings. In the lab I also received great advice from Anouk Evers, Ingrid Brak-Boer, Mariëlle van Grinsven, Hendrik de Buhr and Shuxuan Zheng. Furthermore, I would like to thank the group of Prof. Dr. Jeffrey Beekman, in particular Loes Oosterhoff and Dr. Gimano Amatngalim for their training and tips regarding Air liquid interface culture. I would also like to thank the group of Lukas Kapitein, in particular Dr. Wilco Nijenhuis for his guidance in the process of confocal imaging. In addition, I would like to acknowledge the second reviewer of this thesis Dr. Frank Coenjaerts. Finally, I want to thank the other staff members and students of the MMB department, for a pleasant work atmosphere.

7 Supplementary data

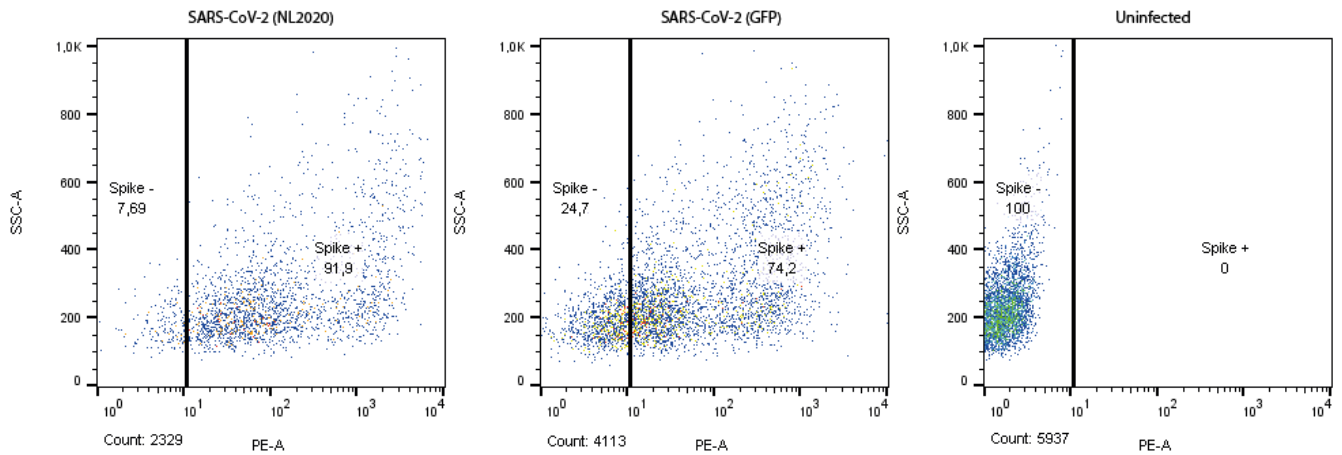


Figure S1: Vero E6 cells are efficiently infected with two strains of SARS-CoV-2 at 2 DPI. Flow cytometric analysis of cell surface SARS-CoV-2 Spike staining (PE) after SARS-CoV-2 infection (NL2020, GFP, MOI 0.05). Gates indicating Spike negative and Spike positive cells were set per cell line and the background PE signal was determined using the uninfected and secondary antibody only controls. The numbers within each gate represent the percentage of the total cell population present in the gate.

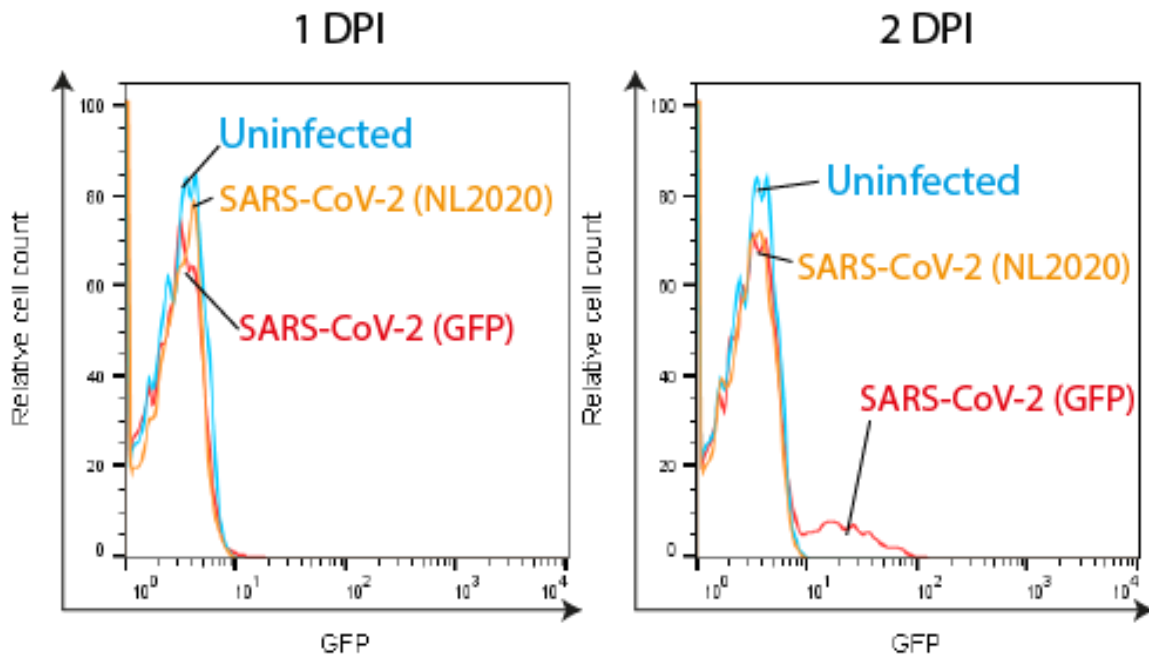


Figure S2: Fluorescence from the SARS-CoV-2 GFP strain is minimally detected using flow cytometry. Flow cytometric analysis of the GFP signal (FITC) in SARS-CoV-2 GFP infected Vero E6 cells (MOI 0.05) at 1 and 2 days post-infection (DPI). Uninfected (Blue), NL2020 infected (orange) and GFP infected (red).

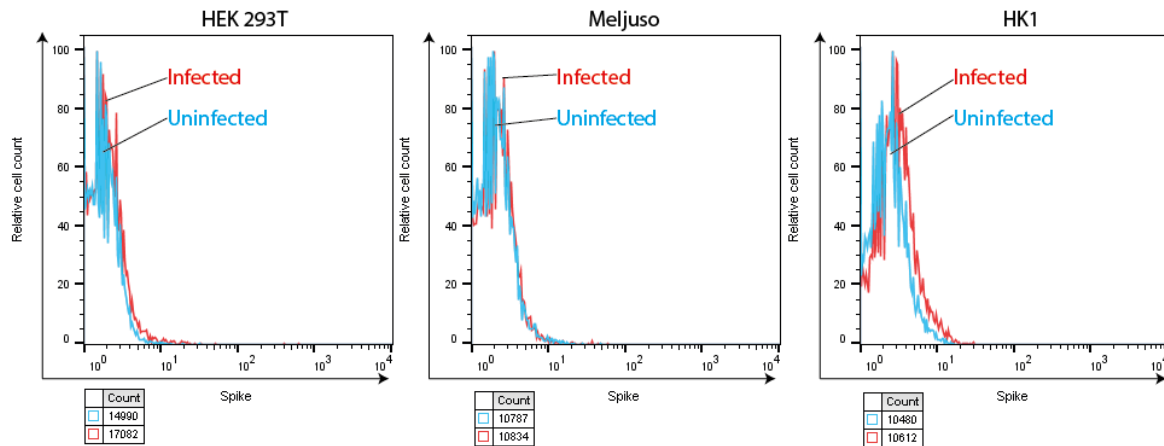


Figure S3: SARS-CoV-2 (NL2020) ineffectively infects human-derived cell lines. Flow cytometric analysis of cell-surface spike-expression in HEK293T, MelJuSo and HK1 cell lines infected with the SARS-CoV-2 NL2020 strain (MOI 0.05). The cells were harvested and analyzed at 2 dpi. Spike-expression on the cell surface was detected by primary anti-spike and secondary PE-conjugated antibodies.

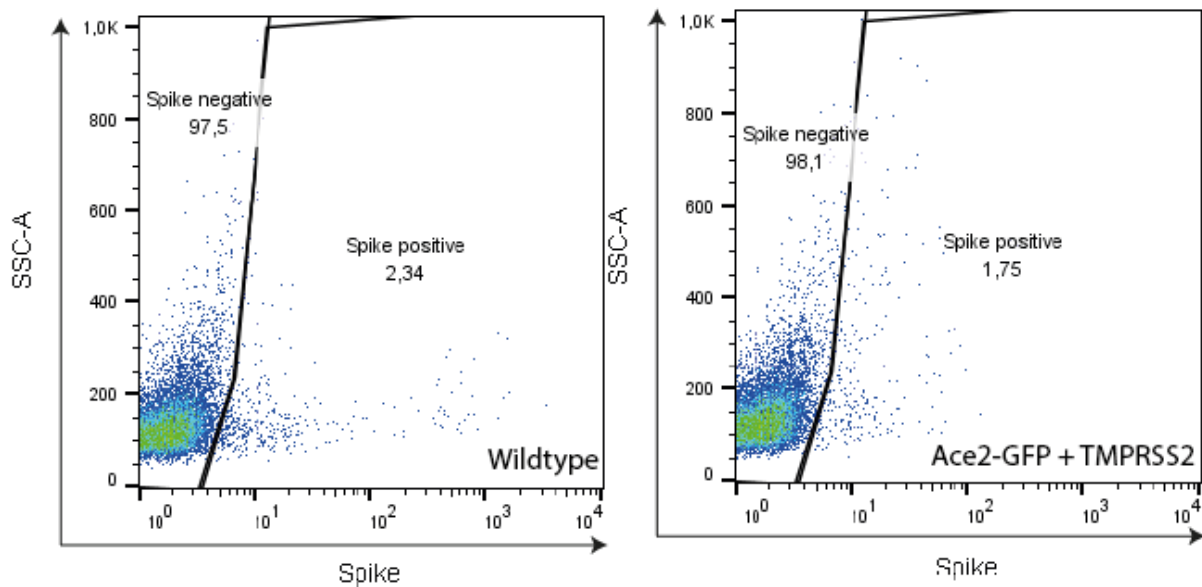


Figure S4: Transduction with SARS-CoV-2 entry factors Ace2 and TMPRSS2 does not increase permissiveness to SARS-CoV-2 infection in HEK293T cells. Flow cytometric analysis of cell-surface spike expression (X-axis) in wildtype and transduced HEK293T cells infected with SARS-CoV-2 (NL2020, MOI 0.05). HEK 293T cells were transduced with lentiviral vectors containing Ace2-GFP and TMPRSS2. Background PE signal was determined using the uninfected and secondary antibody only controls. The numbers within each gate represent the percentage of the total cell population present in the gate.

Cell line	GFP-positive cells after Ace2 transduction and selection	GFP-positive cells after Ace2 transduction, selection and TMPRSS2 transduction
Huh7	58,3 % *	
A549	70,7 %	67,5 %
HEK293T	55,1 %	54,3 %
MeljuSo	65,3 %	64,3 %

*Huh7 was difficult to transduce, and therefore at the timepoint that the other cell lines were transduced with TMPRSS2, Huh7 was not ready to be transduced yet.

Table S1: Transduction efficiency of the Ace2-GFP construct in Huh7, A549, HEK293T and MeljuSo. Cells were transduced with Ace2-GFP and TMPRSS2 constructs and selected with puromycin. GFP-signal shows the percentage of cells containing the Ace2-GFP construct.

References

1. Zhu N, Zhang D, Wang W, et al. A Novel Coronavirus from Patients with Pneumonia in China, 2019. *N Engl J Med*. 2020;382(8). doi:10.1056/nejmoa2001017
2. Peiris JSM, Lai ST, Poon LLM, et al. Coronavirus as a possible cause of severe acute respiratory syndrome. *Lancet*. Published online 2003. doi:10.1016/S0140-6736(03)13077-2
3. Wu Y, Ho W, Huang Y, et al. SARS-CoV-2 is an appropriate name for the new coronavirus. *Lancet*. 2020;395(10228). doi:10.1016/S0140-6736(20)30557-2
4. Hu B, Guo H, Zhou P, Shi ZL. Characteristics of SARS-CoV-2 and COVID-19. *Nat Rev Microbiol*. 2021;19(3). doi:10.1038/s41579-020-00459-7
5. He F, Deng Y, Li W. Coronavirus disease 2019: What we know? *J Med Virol*. 2020;92(7). doi:10.1002/jmv.25766
6. Huang C, Wang Y, Li X, et al. Clinical features of patients infected with 2019 novel coronavirus in Wuhan, China. *Lancet*. Published online 2020. doi:10.1016/S0140-6736(20)30183-5
7. Guan W, Ni Z, Hu Y, et al. Clinical Characteristics of Coronavirus Disease 2019 in China. *N Engl J Med*. Published online 2020. doi:10.1056/nejmoa2002032
8. Wang MY, Zhao R, Gao LJ, Gao XF, Wang DP, Cao JM. SARS-CoV-2: Structure, Biology, and Structure-Based Therapeutics Development. *Front Cell Infect Microbiol*. 2020;10. doi:10.3389/fcimb.2020.587269
9. Wang Y, Wang Y, Chen Y, Qin Q. Unique epidemiological and clinical features of the emerging 2019 novel coronavirus pneumonia (COVID-19) implicate special control measures. *J Med Virol*. Published online 2020. doi:10.1002/jmv.25748
10. Harrison AG, Lin T, Wang P. Mechanisms of SARS-CoV-2 Transmission and Pathogenesis. *Trends Immunol*. 2020;41(12). doi:10.1016/j.it.2020.10.004
11. The Lancet. Facing up to long COVID. *Lancet*. 2020;396(10266). doi:10.1016/S0140-6736(20)32662-3
12. Long COVID: let patients help define long-lasting COVID symptoms. *Nature*. 2020;586(7828). doi:10.1038/d41586-020-02796-2
13. World Economic Forum. *The Global Risks Report 2021: 16th Edition.*; 2021.
14. Johns Hopkins University & Medicine. COVID-19 Map. Johns Hopkins Coronavirus Resource Center.
15. Peiris J, Yuen K, Osterhaus A, Stöhr K. The severe acute respiratory syndrome. *N Engl J Med*. 2003;349:2431-2441.
16. Johansson MA, Quandelacy TM, Kada S, et al. SARS-CoV-2 Transmission From People Without COVID-19 Symptoms Key Points + Supplemental content. *JAMA Netw Open*. Published online 2021.
17. Park JE, Jung S, Kim A. MERS transmission and risk factors: A systematic review. *BMC Public Health*. Published online 2018. doi:10.1186/s12889-018-5484-8
18. Al-Omari A, Rabaan AA, Salih S, Al-Tawfiq JA, Memish ZA. MERS coronavirus outbreak: Implications for emerging viral infections. *Diagn Microbiol Infect Dis*. Published online 2019. doi:10.1016/j.diagmicrobio.2018.10.011
19. Liu Y, Gayle AA, Wilder-Smith A, Rocklöv J. The reproductive number of COVID-19 is higher compared to SARS coronavirus. *J Travel Med*. Published online 2020. doi:10.1093/jtm/taaa021
20. EMA. COVID-19 treatments: authorised. Accessed July 23, 2021. <https://www.ema.europa.eu/en/human-regulatory/overview/public-health-threats/coronavirus-disease-covid-19/treatments-vaccines/treatments-covid-19/covid-19-treatments-authorised>
21. FDA. Know Your Treatment Options for COVID-19. FDA. Published 2021. Accessed July 23, 2021. <https://www.fda.gov/consumers/consumer-updates/know-your-treatment-options-covid-19>
22. NIH. COVID-19 Treatment Guidelines Panel. Coronavirus Disease 2019 (COVID-19) Treatment Guidelines. National Institutes of Health. *Nih*. 2020;2019.
23. Therapeutic Management of Nonhospitalized Adults With COVID-19. Accessed July 23, 2021. <https://www.covid19treatmentguidelines.nih.gov/management/clinical->

- management/nonhospitalized-adults--therapeutic-management/
24. Treatment and pharmaceutical prophylaxis of COVID-19. Accessed July 23, 2021. <https://www.ecdc.europa.eu/en/covid-19/latest-evidence/treatment>
 25. European Medicines Agency. EMA endorses use of dexamethasone in COVID-19 patients on oxygen or mechanical ventilation. 18/9.
 26. Scialo F, Daniele A, Amato F, et al. ACE2: The Major Cell Entry Receptor for SARS-CoV-2. *Lung*. 2020;198(6). doi:10.1007/s00408-020-00408-4
 27. Defendi HGT, da Silva Madeira L, Borschiver S. Analysis of the COVID-19 Vaccine Development Process: an Exploratory Study of Accelerating Factors and Innovative Environments. *J Pharm Innov*. Published online 2021. doi:10.1007/s12247-021-09535-8
 28. Li L, Guo P, Zhang X, Yu Z, Zhang W, Sun H. SARS-CoV-2 vaccine candidates in rapid development. *Hum Vaccines Immunother*. 2021;17(3). doi:10.1080/21645515.2020.1804777
 29. SARS-CoV-2 variants of concern as of 22 July 2021. Accessed July 23, 2021. <https://www.ecdc.europa.eu/en/covid-19/variants-concern>
 30. Su S, Wong G, Shi W, et al. Epidemiology, Genetic Recombination, and Pathogenesis of Coronaviruses. *Trends Microbiol*. Published online 2016. doi:10.1016/j.tim.2016.03.003
 31. Kaur N, Singh R, Dar Z, Bijarnia RK, Dhingra N, Kaur T. Genetic comparison among various coronavirus strains for the identification of potential vaccine targets of SARS-CoV2. *Infect Genet Evol*. Published online 2020. doi:10.1016/j.meegid.2020.104490
 32. Lefkowitz EJ, Dempsey DM, Hendrickson RC, Orton RJ, Siddell SG, Smith DB. Virus taxonomy: The database of the International Committee on Taxonomy of Viruses (ICTV). *Nucleic Acids Res*. Published online 2018. doi:10.1093/nar/gkx932
 33. Woo PCY, Lau SKP, Huang Y, Yuen KY. Coronavirus diversity, phylogeny and interspecies jumping. *Exp Biol Med*. Published online 2009. doi:10.3181/0903-MR-94
 34. Zumla A, Chan JFW, Azhar EI, Hui DSC, Yuen KY. Coronaviruses-drug discovery and therapeutic options. *Nat Rev Drug Discov*. 2016;15(5). doi:10.1038/nrd.2015.37
 35. Centers for Disease Control and Prevention (CDC). Coronavirus | Human Coronavirus Types | CDC. Centers for Disease Control and Prevention.
 36. Lau SKP, Woo PCY, Yip CCY, et al. Coronavirus HKU1 and other coronavirus infections in Hong Kong. *J Clin Microbiol*. Published online 2006. doi:10.1128/JCM.02614-05
 37. Luk HKH, Li X, Fung J, Lau SKP, Woo PCY. Molecular epidemiology, evolution and phylogeny of SARS coronavirus. *Infect Genet Evol*. Published online 2019. doi:10.1016/j.meegid.2019.03.001
 38. Abdallat MM, Abroug F, Al Dhahry SHS, et al. State of knowledge and data gaps of middle east respiratory syndrome coronavirus (MERS-CoV) in humans. *PLoS Curr*. Published online 2013. doi:10.1371/currents.outbreaks.0bf719e352e7478f8ad85fa30127ddb8
 39. Zhou P, Yang X Lou, Wang XG, et al. A pneumonia outbreak associated with a new coronavirus of probable bat origin. *Nature*. Published online 2020. doi:10.1038/s41586-020-2012-7
 40. Cui J, Li F, Shi ZL. Origin and evolution of pathogenic coronaviruses. *Nat Rev Microbiol*. Published online 2019. doi:10.1038/s41579-018-0118-9
 41. Zheng J. SARS-coV-2: An emerging coronavirus that causes a global threat. *Int J Biol Sci*. Published online 2020. doi:10.7150/ijbs.45053
 42. Li X, Zai J, Zhao Q, et al. Evolutionary history, potential intermediate animal host, and cross-species analyses of SARS-CoV-2. *J Med Virol*. Published online 2020. doi:10.1002/jmv.25731
 43. Lu R, Zhao X, Li J, et al. Genomic characterisation and epidemiology of 2019 novel coronavirus: implications for virus origins and receptor binding. *Lancet*. Published online 2020. doi:10.1016/S0140-6736(20)30251-8
 44. Cavanagh D, Britton P. Coronaviruses: General Features. In: *Encyclopedia of Virology*. ; 2008. doi:10.1016/B978-012374410-4.00370-8
 45. Walls AC, Park YJ, Tortorici MA, Wall A, McGuire AT, Veesler D. Structure, Function, and Antigenicity of the SARS-CoV-2 Spike Glycoprotein. *Cell*. 2020;181(2). doi:10.1016/j.cell.2020.02.058
 46. V'kovski P, Kratzel A, Steiner S, Stalder H, Thiel V. Coronavirus biology and replication:

- implications for SARS-CoV-2. *Nat Rev Microbiol.* 2021;19(3). doi:10.1038/s41579-020-00468-6
47. Wrapp D, Wang N, Corbett KS, et al. Cryo-EM structure of the 2019-nCoV spike in the prefusion conformation. *Science (80-).* 2020;367(6483). doi:10.1126/science.aax0902
 48. Wang Q, Zhang Y, Wu L, et al. Structural and Functional Basis of SARS-CoV-2 Entry by Using Human ACE2. *Cell.* 2020;181(4). doi:10.1016/j.cell.2020.03.045
 49. Stancioiu F, Papadakis GZ, Kteniadakis S, et al. A dissection of SARS-CoV2 with clinical implications (Review). *Int J Mol Med.* 2020;46(2). doi:10.3892/ijmm.2020.4636
 50. Xia S, Liu M, Wang C, et al. Inhibition of SARS-CoV-2 (previously 2019-nCoV) infection by a highly potent pan-coronavirus fusion inhibitor targeting its spike protein that harbors a high capacity to mediate membrane fusion. *Cell Res.* 2020;30(4). doi:10.1038/s41422-020-0305-x
 51. Glowacka I, Bertram S, Muller MA, et al. Evidence that TMPRSS2 Activates the Severe Acute Respiratory Syndrome Coronavirus Spike Protein for Membrane Fusion and Reduces Viral Control by the Humoral Immune Response. *J Virol.* 2011;85(9). doi:10.1128/jvi.02232-10
 52. Simmons G, Gosalia DN, Rennekamp AJ, Reeves JD, Diamond SL, Bates P. Inhibitors of cathepsin L prevent severe acute respiratory syndrome coronavirus entry. *Proc Natl Acad Sci U S A.* 2005;102(33). doi:10.1073/pnas.0505577102
 53. Hoffmann M, Kleine-Weber H, Schroeder S, et al. SARS-CoV-2 Cell Entry Depends on ACE2 and TMPRSS2 and Is Blocked by a Clinically Proven Protease Inhibitor. *Cell.* 2020;181(2). doi:10.1016/j.cell.2020.02.052
 54. Bestle D, Heindl MR, Limburg H, et al. TMPRSS2 and furin are both essential for proteolytic activation of SARS-CoV-2 in human airway cells. *Life Sci Alliance.* 2020;3(9). doi:10.26508/LSA.202000786
 55. Johnson BA, Xie X, Kalveram B, et al. Furin Cleavage Site Is Key to SARS-CoV-2 Pathogenesis. *bioRxiv Prepr Serv Biol.* Published online 2020. doi:10.1101/2020.08.26.268854
 56. Hoffmann M, Kleine-Weber H, Pöhlmann S. A Multibasic Cleavage Site in the Spike Protein of SARS-CoV-2 Is Essential for Infection of Human Lung Cells. *Mol Cell.* 2020;78(4). doi:10.1016/j.molcel.2020.04.022
 57. Coutard B, Valle C, de Lamballerie X, Canard B, Seidah NG, Decroly E. The spike glycoprotein of the new coronavirus 2019-nCoV contains a furin-like cleavage site absent in CoV of the same clade. *Antiviral Res.* 2020;176. doi:10.1016/j.antiviral.2020.104742
 58. Gkogkou E, Barnasas G, Vougas K, Trougakos IP. Expression profiling meta-analysis of ACE2 and TMPRSS2, the putative anti-inflammatory receptor and priming protease of SARS-CoV-2 in human cells, and identification of putative modulators. *Redox Biol.* 2020;36. doi:10.1016/j.redox.2020.101615
 59. Lukassen S, Chua RL, Trefzer T, et al. SARS-CoV-2 receptor ACE2 and TMPRSS2 are primarily expressed in bronchial transient secretory cells. *EMBO J.* Published online 2020. doi:10.15252/embj.2020105114
 60. Kim D, Lee JY, Yang JS, Kim JW, Kim VN, Chang H. The Architecture of SARS-CoV-2 Transcriptome. *Cell.* 2020;181(4). doi:10.1016/j.cell.2020.04.011
 61. Chan JFW, Kok KH, Zhu Z, et al. Genomic characterization of the 2019 novel human-pathogenic coronavirus isolated from a patient with atypical pneumonia after visiting Wuhan. *Emerg Microbes Infect.* 2020;9(1). doi:10.1080/22221751.2020.1719902
 62. Romano M, Ruggiero A, Squeglia F, Maga G, Berisio R. A Structural View of SARS-CoV-2 RNA Replication Machinery: RNA Synthesis, Proofreading and Final Capping. *Cells.* 2020;9(5). doi:10.3390/cells9051267
 63. Iserman C, Roden C, Boerneke M, et al. Specific viral RNA drives the SARS CoV-2 nucleocapsid to phase separate. *bioRxiv Prepr Serv Biol.* Published online 2020. doi:10.1101/2020.06.11.147199
 64. Ravi M, Paramesh V, Kaviya SR, Anuradha E, Paul Solomon FD. 3D cell culture systems: Advantages and applications. *J Cell Physiol.* 2015;230(1). doi:10.1002/jcp.24683
 65. Yu M, Selvaraj SK, Liang-Chu MMY, et al. A resource for cell line authentication, annotation and quality control. *Nature.* 2015;520(7547). doi:10.1038/nature14397

66. Takayama K. In Vitro and Animal Models for SARS-CoV-2 research. *Trends Pharmacol Sci.* 2020;41(8). doi:10.1016/j.tips.2020.05.005
67. Matsuyama S, Nao N, Shirato K, et al. Enhanced isolation of SARS-CoV-2 by TMPRSS2-expressing cells. *Proc Natl Acad Sci U S A.* 2020;117(13). doi:10.1073/pnas.2002589117
68. Jang H, Ross TM. Dried SARS-CoV-2 virus maintains infectivity to Vero E6 cells for up to 48 h. *Vet Microbiol.* 2020;251. doi:10.1016/j.vetmic.2020.108907
69. Desmyter J, Melnick JL, Rawls WE. Defectiveness of Interferon Production and of Rubella Virus Interference in a Line of African Green Monkey Kidney Cells (Vero). *J Virol.* 1968;2(10). doi:10.1128/jvi.2.10.955-961.1968
70. Naoki O, Arihiro K, Toshiyuki Y, et al. The genome landscape of the African Green Monkey kidney-derived vero cell line. *DNA Res.* 2014;21(6). doi:10.1093/dnares/dsu029
71. Ren X, Glende J, Al-Falah M, et al. Analysis of ACE2 in polarized epithelial cells: Surface expression and function as receptor for severe acute respiratory syndrome-associated coronavirus. *J Gen Virol.* 2006;87(6). doi:10.1099/vir.0.81749-0
72. Ogando NS, Dalebout TJ, Zevenhoven-Dobbe JC, et al. SARS-coronavirus-2 replication in Vero E6 cells: Replication kinetics, rapid adaptation and cytopathology. *J Gen Virol.* 2020;101(9). doi:10.1099/jgv.0.001453
73. Davidson AD, Williamson MK, Lewis S, et al. Characterisation of the transcriptome and proteome of SARS-CoV-2 reveals a cell passage induced in-frame deletion of the furin-like cleavage site from the spike glycoprotein. *Genome Med.* 2020;12(1). doi:10.1186/s13073-020-00763-0
74. Lau SY, Wang P, Mok BWY, et al. Attenuated SARS-CoV-2 variants with deletions at the S1/S2 junction. *Emerg Microbes Infect.* 2020;9(1). doi:10.1080/22221751.2020.1756700
75. Ramirez S, Fernandez-Antunez C, Galli A, et al. Overcoming culture restriction for SARS-CoV-2 in human cells facilitates the screening of compounds inhibiting viral replication. *Antimicrob Agents Chemother.* Published online 2021. doi:10.1128/aac.00097-21
76. Laranger R, Peters-Hall JR, Coquelin M, et al. Reconstituting Mouse Lungs with Conditionally Reprogrammed Human Bronchial Epithelial Cells. *Tissue Eng - Part A.* 2018;24(7-8). doi:10.1089/ten.tea.2017.0114
77. Gentzsch M, Boyles SE, Cheluvvaraju C, et al. Pharmacological rescue of conditionally reprogrammed cystic fibrosis bronchial epithelial cells. *Am J Respir Cell Mol Biol.* 2017;56(5). doi:10.1165/rcmb.2016-0276MA
78. Lam HC, Choi AMK, Ryter SW. Isolation of mouse respiratory epithelial cells and exposure to experimental cigarette smoke at air liquid interface. *J Vis Exp.* 2010;(48). doi:10.3791/2513
79. Clevers H. Modeling Development and Disease with Organoids. *Cell.* 2016;165(7). doi:10.1016/j.cell.2016.05.082
80. Salahudeen AA, Choi SS, Rustagi A, et al. Progenitor identification and SARS-CoV-2 infection in human distal lung organoids. *Nature.* 2020;588(7839). doi:10.1038/s41586-020-3014-1
81. He B, Chen G, Zeng Y. Three-dimensional cell culture models for investigating human viruses. *Virol Sin.* 2016;31(5). doi:10.1007/s12250-016-3889-z
82. Crawford KHD, Eguia R, Dingens AS, et al. Protocol and reagents for pseudotyping lentiviral particles with SARS-CoV-2 spike protein for neutralization assays. *Viruses.* 2020;12(5). doi:10.3390/v12050513
83. Gordon DE, Jang GM, Bouhaddou M, et al. A SARS-CoV-2 protein interaction map reveals targets for drug repurposing. *Nature.* 2020;583(7816). doi:10.1038/s41586-020-2286-9
84. Yadav V, Panganiban AT, Honer Zu Bentrup K, Voss TG. Influenza infection modulates vesicular trafficking and induces Golgi complex disruption. *VirusDisease.* 2016;27(4). doi:10.1007/s13337-016-0347-3
85. Beske O, Reichelt M, Taylor MP, Kirkegaard K, Andino R. Poliovirus infection blocks ERGIC-to-Golgi trafficking and induces microtubule-dependent disruption of the Golgi complex. *J Cell Sci.* 2007;120(18). doi:10.1242/jcs.03483
86. Campadelli G, Brandimarti R, Di Lazzaro C, Ward PL, Roizman B, Torrisi MR. Fragmentation and

- dispersal of Golgi proteins and redistribution of glycoproteins and glycolipids processed through the Golgi apparatus after infection with herpes simplex virus 1. *Proc Natl Acad Sci U S A*. 1993;90(7). doi:10.1073/pnas.90.7.2798
87. Chu H, Chan JF-W, Yuen TT-T, et al. Comparative tropism, replication kinetics, and cell damage profiling of SARS-CoV-2 and SARS-CoV with implications for clinical manifestations, transmissibility, and laboratory studies of COVID-19: an observational study. *The Lancet Microbe*. 2020;1(1). doi:10.1016/s2666-5247(20)30004-5
 88. Sanclemente-Alaman I, Moreno-Jiménez L, Benito-Martín MS, et al. Experimental Models for the Study of Central Nervous System Infection by SARS-CoV-2. *Front Immunol*. 2020;11. doi:10.3389/fimmu.2020.02163
 89. de Lang A, Osterhaus ADME, Haagmans BL. Interferon- γ and interleukin-4 downregulate expression of the SARS coronavirus receptor ACE2 in Vero E6 cells. *Virology*. 2006;353(2). doi:10.1016/j.virol.2006.06.011
 90. Wei J, Alfajaro MM, DeWeirdt PC, et al. Genome-wide CRISPR Screens Reveal Host Factors Critical for SARS-CoV-2 Infection. *Cell*. 2021;184(1). doi:10.1016/j.cell.2020.10.028
 91. Bonser LR, Koh KD, Johansson K, et al. Flow-cytometric analysis and purification of airway epithelial-cell subsets. *Am J Respir Cell Mol Biol*. 2021;64(3). doi:10.1165/rcmb.2020-0149MA
 92. Konda B, Mulay A, Yao C, Beil S, Israely E, Stripp BR. Isolation and enrichment of human lung epithelial progenitor cells for organoid culture. *J Vis Exp*. 2020;2020(161). doi:10.3791/61541
 93. Berryman M, Franck Z, Bretscher A. Ezrin is concentrated in the apical microvilli of a wide variety of epithelial cells whereas moesin is found primarily in endothelial cells. *J Cell Sci*. 1993;105(4). doi:10.1242/jcs.105.4.1025
 94. Nijenhuis W, Damstra HGJ, Grinsven EJ van, et al. Optical nanoscopy reveals SARS-CoV-2-induced remodeling of human airway cells. *bioRxiv*. Published online 2021.
 95. Verkhivker GM, Agajanian S, Oztas DY, Gupta G. Comparative Perturbation-Based Modeling of the SARS-CoV-2 Spike Protein Binding with Host Receptor and Neutralizing Antibodies: Structurally Adaptable Allosteric Communication Hotspots Define Spike Sites Targeted by Global Circulating Mutations. *Biochemistry*. Published online 2021. doi:10.1021/acs.biochem.1c00139
 96. Choy KT, Wong AYL, Kaewpreedee P, et al. Remdesivir, lopinavir, emetine, and homoharringtonine inhibit SARS-CoV-2 replication in vitro. *Antiviral Res*. 2020;178. doi:10.1016/j.antiviral.2020.104786
 97. Pohl MO, Busnadiego I, Kufner V, et al. SARS-CoV-2 variants reveal features critical for replication in primary human cells. *PLOS Biol*. 2021;19(3). doi:10.1371/journal.pbio.3001006
 98. Bielarz V, Willemart K, Avalosse N, et al. Susceptibility of neuroblastoma and glioblastoma cell lines to SARS-CoV-2 infection. *Brain Res*. 2021;1758. doi:10.1016/j.brainres.2021.147344
 99. Park BK, Kim D, Park S, et al. Differential signaling and virus production in calu-3 cells and vero cells upon sars-cov-2 infection. *Biomol Ther*. 2021;29(3). doi:10.4062/biomolther.2020.226
 100. Cuevas JM, Durán-Moreno M, Sanjuán R. Multi-virion infectious units arise from free viral particles in an enveloped virus. *Nat Microbiol*. 2017;2. doi:10.1038/nmicrobiol.2017.78
 101. Case JB, Bailey AL, Kim AS, Chen RE, Diamond MS. Growth, detection, quantification, and inactivation of SARS-CoV-2. *Virology*. 2020;548. doi:10.1016/j.virol.2020.05.015
 102. Mendoza EJ, Manguiat K, Wood H, Drebot M. Two Detailed Plaque Assay Protocols for the Quantification of Infectious SARS-CoV-2. *Curr Protoc Microbiol*. 2020;57(1). doi:10.1002/cpmc.105
 103. ATCC® *VIROLOGY GUIDE*; 2016. Accessed September 10, 2021. <https://www.atcc.org/-/media/resources/culture-guides/virology-guide.pdf?rev=a3816afe46cb499c90265fcf6456d2e3>
 104. Bryan WR. INTERPRETATION OF HOST RESPONSE IN QUANTITATIVE STUDIES ON ANIMAL VIRUSES. *Ann N Y Acad Sci*. 1957;69(4). doi:10.1111/j.1749-6632.1957.tb49710.x
 105. Wulff NH, Tzatzaris M, Young PJ. Monte Carlo simulation of the Spearman-Kaerber TCID50. *J Clin Bioinforma*. 2012;2(1). doi:10.1186/2043-9113-2-5
 106. Smither SJ, Lear-Rooney C, Biggins J, Pettitt J, Lever MS, Olinger GG. Comparison of the plaque

- assay and 50% tissue culture infectious dose assay as methods for measuring filovirus infectivity. *J Virol Methods*. 2013;193(2). doi:10.1016/j.jviromet.2013.05.015
107. Kimura T, Ohno N, Terada N, et al. Hepatitis B virus DNA-negative dane particles lack core protein but contain a 22-kDa precore protein without C-terminal arginine-rich domain. *J Biol Chem*. 2005;280(23). doi:10.1074/jbc.M501564200
 108. Jacobs NT, Onuoha NO, Antia A, Steel J, Antia R, Lowen AC. Incomplete influenza A virus genomes occur frequently but are readily complemented during localized viral spread. *Nat Commun*. 2019;10(1). doi:10.1038/s41467-019-11428-x
 109. Reta A. Defective Interfering Particles and Their Role in Disease Progression and Persistence. *Arch Microbiol Immunol*. 2017;01(02). doi:10.26502/ami.9365009
 110. Alexandersen S, Chamings A, Bhatta TR. SARS-CoV-2 genomic and subgenomic RNAs in diagnostic samples are not an indicator of active replication. *Nat Commun*. 2020;11(1). doi:10.1038/s41467-020-19883-7
 111. Stewart JC, Villasmil ML, Frampton MW. Changes in fluorescence intensity of selected leukocyte surface markers following fixation. *Cytom Part A*. 2007;71(6). doi:10.1002/cyto.a.20392
 112. Daniloski Z, Jordan TX, Wessels HH, et al. Identification of Required Host Factors for SARS-CoV-2 Infection in Human Cells. *Cell*. 2021;184(1). doi:10.1016/j.cell.2020.10.030
 113. Cortese M, Lee JY, Cerikan B, et al. Integrative Imaging Reveals SARS-CoV-2-Induced Reshaping of Subcellular Morphologies. *Cell Host Microbe*. 2020;28(6). doi:10.1016/j.chom.2020.11.003
 114. Kulkarni-Gosavi P, Makhoul C, Gleeson PA. Form and function of the Golgi apparatus: scaffolds, cytoskeleton and signalling. *FEBS Lett*. 2019;593(17). doi:10.1002/1873-3468.13567
 115. Bouhaddou M, Memon D, Meyer B, et al. The Global Phosphorylation Landscape of SARS-CoV-2 Infection. *Cell*. 2020;182(3). doi:10.1016/j.cell.2020.06.034
 116. Wang M, Cao R, Zhang L, et al. Remdesivir and chloroquine effectively inhibit the recently emerged novel coronavirus (2019-nCoV) in vitro. *Cell Res*. 2020;30(3). doi:10.1038/s41422-020-0282-0
 117. Skipper CP, Pastick KA, Engen NW, et al. Hydroxychloroquine in Nonhospitalized Adults With Early COVID-19: A Randomized Trial. *Ann Intern Med*. 2020;173(8). doi:10.7326/M20-4207
 118. "The RECOVERY Collaborative Group." Effect of Hydroxychloroquine in Hospitalized Patients with Covid-19. *N Engl J Med*. 2020;383(21). doi:10.1056/NEJMoa2022926
 119. Ou T, Mou H, Zhang L, Ojha A, Choe H, Farzan M. Hydroxychloroquine-mediated inhibition of SARS-CoV-2 entry is attenuated by TMPRSS2. *PLoS Pathog*. 2021;17(1 January). doi:10.1371/journal.ppat.1009212
 120. Savarino A, Boelaert JR, Cassone A, Majori G, Cauda R. Effects of chloroquine on viral infections: An old drug against today's diseases? *Lancet Infect Dis*. 2003;3(11). doi:10.1016/S1473-3099(03)00806-5
 121. Saul S, Karim M, Huang P-T, et al. Discovery of pan-ErbB inhibitors protecting from SARS-CoV-2 replication, inflammation, and lung injury by a drug repurposing screen. *bioRxiv*. Published online 2021.
 122. Xia H, Cao Z, Xie X, et al. Evasion of Type I Interferon by SARS-CoV-2. *Cell Rep*. 2020;33(1). doi:10.1016/j.celrep.2020.108234
 123. Zhang Y, Chen Y, Li Y, et al. The ORF8 protein of SARS-CoV-2 mediates immune evasion through down-regulating MHC-I. *Proc Natl Acad Sci*. 2021;118(23). doi:10.1073/pnas.2024202118
 124. García LF. Immune Response, Inflammation, and the Clinical Spectrum of COVID-19. *Front Immunol*. 2020;11. doi:10.3389/fimmu.2020.01441
 125. Thélu A, Catoire S, Kerdine-Römer S. Immune-competent in vitro co-culture models as an approach for skin sensitisation assessment. *Toxicol Vitro*. 2020;62. doi:10.1016/j.tiv.2019.104691
 126. Gottfried E, Kunz-Schughart LA, Andreesen R, Kreutz M. Brave little world: Spheroids as an in vitro model to study tumor-immune-cell interactions. *Cell Cycle*. 2006;5(7). doi:10.4161/cc.5.7.2624
 127. Tang H, Abouleila Y, Si L, et al. Human Organs-on-Chips for Virology. *Trends Microbiol*.

